NASA CR- 86020

STUDY OF SOLID LASER MATERIALS

By F. C. Unterleitner and H. Banerjee

FINAL REPORT

June 1967

Prepared under Contract No. NAS 12-120,
Control No. ERC/R&D 66-531, by

Research and Advanced Technology Department
ELECTRONICS DIVISION OF GENERAL DYNAMICS
Rochester, New York

Prepared for

NATIONAL AERONAUTICS AND SPACE ADMINISTRATION
Electronics Research Center
Space Optics Laboratory

TABLE OF CONTENTS

LIST OF ILLUSTRATIONS

SUMMARY

The investigations reported here aim at improving understanding of the excellent optically pumped laser material Nd^{3+}:YAG. An attempt was made to find a unique set of crystal field parameters which would permit calculation of eigenfunctions and eigenvalues for $4f^n$ electron configurations of rare earth ions in yttrium aluminum garnet, particularly those below 14,000 cm^{-1}. The simpler case of Yb^{3+}:YAG having $4f^{13}$ (one hole) configuration was treated first. Because of the simplicity of the ground state wave functions, it was possible to show that no set of crystal field parameters is compatible with both the $^2F_{7/2}$ and $^2F_{5/2}$ eigenvalues, if no mixing is permitted between the two manifolds. This unexpected negative result prevented the carrying out of the remainder of the program, but it is believed to have implications with respect to the applicability of crystal field theory in analysis of bound electronic states in crystals.

A scanning spectrometer for recording the absorption spectra of optically pumped materials was developed. The instrument has a spectral resolution of about 3 Å throughout the near ultraviolet, visible, and near infrared spectrum. The time resolution is about 15 μsec, and delay from the pump flash is adjustable. Pump pulse repetition rate is 0.1 per sec. The instrument was tested by examining parts of the ordinary ray metastable state absorption of ruby, showing good agreement with previous measurements. The metastable state absorption spectrum of Nd^{3+}:YAG was measured between 10,000 cm^{-1} and 30,000 cm^{-1}. A few sharp absorption lines were observed which correspond to transitions to states also observed in the ground state absorption. In addition, a continuum of metastable state absorption having a cross section of about 4×10^{-21} cm^2 in the visible spectrum was observed. Removal of pump lamp energy at wavelengths shorter than 5000 Å for continuous wave Nd^{3+}: YAG lasers is recommended on the basis of this continuum metastable state absorption.

INTRODUCTION

PREVIOUS INVESTIGATION

The research reported here is a continuation of research on optically pumped laser materials. Most of the problems to be considered were initially encountered during a study of the influence of magnetic fields on

ruby and neodymium doped Yttrium Aluminum Garnet (Nd : YAG) laser emission performed under a previous contract.[1]

The results of experiments on frequency shifts of laser emission from Nd : YAG in the presence of a magnetic field could not be interpreted. A more comprehensive study of the Zeeman effect in that laser material appeared to be appropriate since nothing has been published on it, to our knowledge. D. L. Wood of Bell Laboratories indicated that he has done some experimental work on Zeeman splitting in that material but was not able to interpret it satisfactorily and has not published the results.

In another phase of the above mentioned program,[1] the influence of the absorption from ions in the metastable states of ruby was measured. This study has been refined somewhat as a result of more recent investigations.[2, 3, 4] The results suggest that a similar study of the Nd : YAG material would be in order.

PROBLEM AREAS INVESTIGATED

Theoretical Treatment of Energy Levels of Ions in Crystals

The absorption lines encountered in the visible and near infrared spectrum of Nd^{3+} : YAG are associated with the neodymium ions since pure YAG is transparent in that region of the spectrum. Koningstein and Geusic[5] were able to assign most of the absorption lines to known free ion terms, but their procedure and the results as to finding the crystal field parameters are not very satisfactory. In this study, the planned approach to the case of Nd^{3+} in YAG was through the simpler case of Yb^{3+} in YAG. It was desired to find the crystal field utilizing the fact that the unique number of parameters needed is decided by the degrees of freedom of the system (this is essentially model dependent) and that the interconnections of the crystal field matrix elements in one j-orbit with those in another are governed by the point group symmetry at the ion site. If a unique crystal potential can be found, one could treat the two- and three-electron (or hole) systems with the same crystal field. It was, of course, anticipated that modifications may have to be made to the parameters to take into account the varying local distortions produced by introducing various rare earth ions at the yttrium site, but it was believed that the uniqueness of the derivation of the parameters for Yb^{3+}: YAG would help in understanding any such minor adjustments.

Carrying out this objective, however, was prevented by the rather unexpected result that no crystal field could be found which, under certain simplifying conditions, was compatible with the observed Yb^{3+} spectrum. The calculation and its interpretation are discussed in detail in the following section.

Metastable State Absorption

An optically pumped laser material may be considered as an intimate mixture of bound electronic systems of two types, the normal ground state system and the metastable state system. Both systems are nearly in thermal equilibrium with the heat bath because of strong coupling to the thermal vibrations of the matrix material but are more weakly coupled to each other through radiative absorption, spontaneous emission, and stimulated emission. Since considerable population density must exist in both systems under conditions of laser operation, the absorption spectrum of the metastable state can strongly influence laser operation. As pointed out in Ref. 4 there are two ways in which metastable state absorption influences laser operation. First, absorption within the frequency band of laser gain serves to reduce available gain; second, absorption within the incident pumping spectrum reduces pump intensity inside the laser rod and provides an additional source of heat input to the laser material. All these effects are detrimental to laser operation and are minimized by the proper choice of laser medium and, once a medium has been selected, judicious restriction of the pump lamp spectrum incident on the laser rod. For the case of Nd^{3+}: YAG, most of the metastable state line absorption is expected to be in the infrared, but there may also be continuum absorption, such as is noted for the ground state at wavelenghts shorter than about 4500 Å. The technique developed for obtaining this spectral information is discussed later in this report, along with the results of measurements made on ruby and Nd: YAG up to the end of the contract period.

THEORY

OUTLINE OF THE Yb^{3+}: YAG PROBLEM

The properties of the rare-earth ions in the garnet lattice have been studied[6, 7] by assuming that the effect of the diamagnetic lattice-environment at the ion-site can be represented by an electrostatic crystal field. This latter quantity is usually expanded in terms of spherical harmonics and treated as a perturbation on the free-ion states. Its salient feature is removal of degeneracy due to the rotational invariance. Parity considerations, angular momentum selection rules, and the (point-group) symmetry at the ion-site decide which of the spherical harmonic terms should be included. Since the crystal field is a one-electron potential, one of its simplest application is in the case of Yb^{3+} ion, which has one hole in the 4f shell. Furthermore, the spin-orbit splitting of the $j = 5/2$ and the $j = 7/2$ multiplets in Yb^{3+}: YAG is an order of magnitude larger than the observed crystal splittings. This leads to the hypothesis that there is almost no admixture caused by the crystal field between the two multiplets.

Thus for Yb^{3+} in a D_2 site one deduces that:

(a) The $j = 7/2$ manifold splits into four levels and the $j = 5/2$ manifold into three levels, the $+m$ and $-m$ states of the same j-orbit (the Kramer's doublets), in systems of odd electron numbers, are still degenerate as a result of the time-reversal invariance of the Hamiltonian;

(b) There are nine different spherical harmonic terms allowed in the crystal potential.

Under an external magnetic field the Kramer's doublets will split up, giving added information about the system. For Yb^{3+}: YAG, however, only the splitting of the lowest level of each of the two manifolds is accurately known. The Hamiltonian to be used to fit the experimental data can now be written as follows:

$$H = H_{\text{spin-orbit}} + H_{\text{crystal}} + \mu_B \vec{H} \cdot (\vec{L} + 2\vec{S}). \qquad (1)$$

In the right-hand side, the contributions are in descending order of magnitude counting terms from the left to the right.

$$H_{\text{crystal}} = \sum_{k\,q} a_q^k \, Y_q^k, \qquad (2)$$

where Y_q^k is a spherical harmonic tensor of rank k and magnetic projection q, and the a's are parameters. For D_2 group, allowed (kq)'s are

$$\begin{array}{llll} k=6, & q=0, & \pm 2, & \pm 4, \pm 6 \\ k=4, & q=0, & \pm 2, & \pm 4 \\ k=2, & q=0, & \pm 2 & \end{array} \qquad (3)$$

and $a_q^k = a_{-q}^k$.

In the third term, $\vec{H}$ stands for the external magnetic field. The rest are in the usual notations.

Experimentally, however, many more lines than can be accounted for by the above mentioned analysis are observed. As a result, a degree of obscurity and arbitrariness persisted in picking out the pure (!) electronic lines. The study described in Ref. 8 seems to have eliminated this arbitrariness. In any case, the data quoted therein form the basis of the present study. (See Fig. 1)

Chronologically speaking, the first complete theoretical calculation was by Hutchings and Wolf.[9] They carried out a point-charge model calculation, summing the contributions of many neighboring ions. Their prediction of levels disagreed sharply with the experimental assignments available at that time[10] and was remarkably in the right direction, judging from the viewpoint of later experiments. (See Fig. 2.)

In the present study no attempt is made to derive the parameters "a_q^k" either from the basic principles of the point-charge model or to obtain the best fit of the parameters by straight-forward calculations. Instead it is noted that, if it is true that there is no admixture of the $j = 5/2$ and $j = 7/2$ manifolds and that the same interaction is manifested in the two manifolds, then the degrees of freedom of the system are four in number (larger of the two j's + 1/2). Knowing the matrix elements of the 4 x 4 secular matrix in the $j = 7/2$ manifold (altogether nine of them if the secular matrix is taken to be traceless, thus incorporating the fact that the crystal potential merely splits up the manifold with the center of gravity of the spectrum at the free ionic level) one can determine by Racah algebra the a_q^k coefficients and hence calculate the matrix elements of the $j = 5/2$ manifold (this secular matrix will be automatically traceless again). If it was now possible to correlate the former nine matrix elements with the experimentally observed four energy eigenvalues and the ground state g-values (this correlation is not a-priori one-to-one), then one could also correlate the five matrix elements of $j = 5/2$ manifold terms of the experimental quantities of

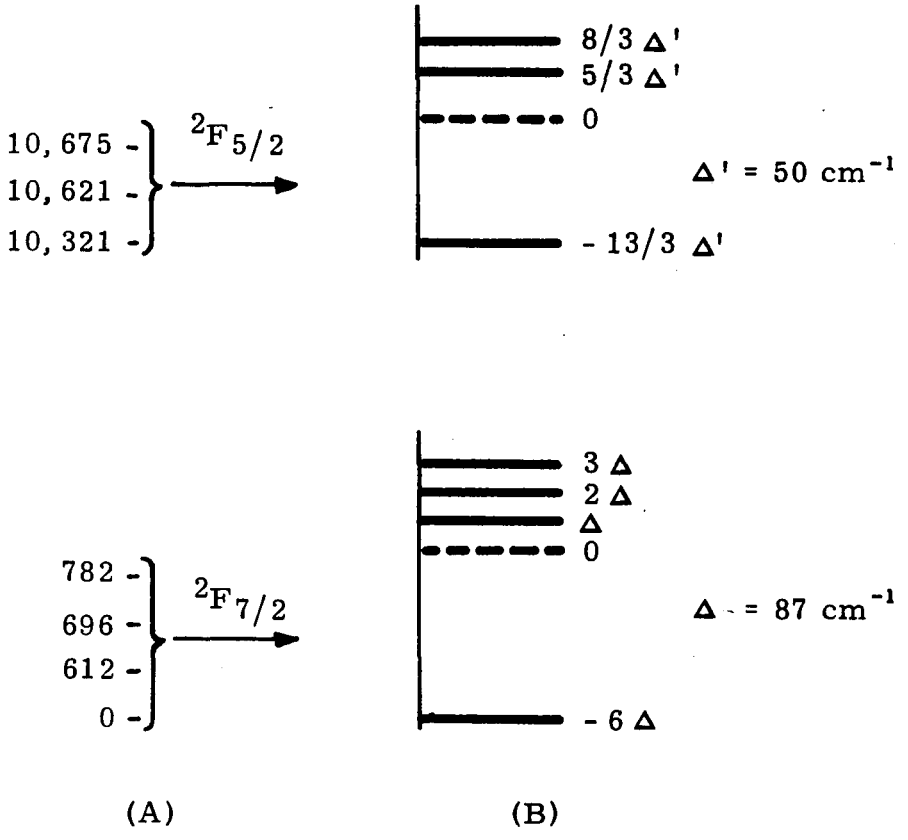

(A) Level positions written down for Yb^{3+}: YAG. Scale is in cm^{-1}. Measurements of Pearson, et al. [8]

(B) Each of the manifolds represented with centroid at zero in a convenient scale.

Fig. 1. Energy levels of Yb^{3+}:YAG.

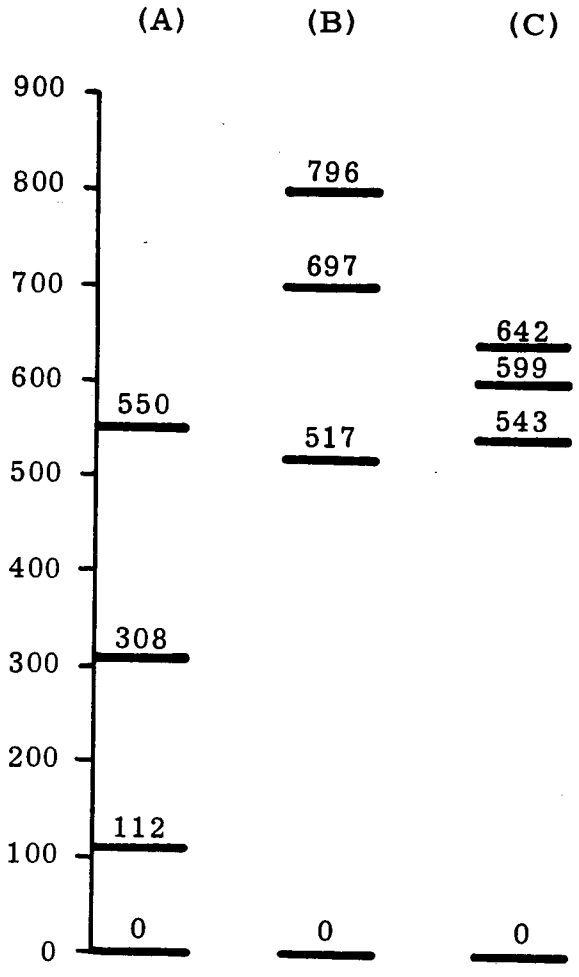

Lower Four Levels of Yb:YGaG

(A) Measurements of Wood.[10]
(B) Calculations of Hutchings and Wolf.[9]
(C) Measurements of Pearson, et al.[8]

Fig. 2. Experimental and theoretical situations for Yb^{3+}:YGaG.

the j = 7/2 manifold. Demanding that the three observed energy levels of the j = 5/2 manifold be reproduced, the functional forms and the values of all the matrix elements could be uniquely settled. Unfortunately, this kind of correlation involves the inverse process of matrix diagonalization, given the eigenvalues and the ground state g-values, and is generally not practical. But it is shown that the problem is solvable if one assumes a ground state structure (suggested and used by Koster and Statz)[11] that yields the observed g-values and satisfies some broad theoretical requirements. Calculations carried out according to the above outline do not show that any crystal potential exists that could even crudely fit the experimental data. Various underlying assumptions, uncertainties, and alternatives are discussed.

GROUP THEORETICAL CONSIDERATIONS AND THE GROUND STATE STRUCTURE

It is known[12] that the (2j+1) dimensional irreducible representation of the rotation group, designated by the label of angular momentum j, breaks up into j + 1/2, two-dimensional Γ_5 irreducible representations of the D_2 group. The spinor

$$\begin{pmatrix} |1/2\ \ 1/2> \\ |1/2\text{-}1/2> \end{pmatrix} \tag{4}$$

transforms according to this Γ_5 irreducible representation of D_2. For j = 7/2 orbit, we then have this Γ_5 irreducible representation coming in with the multiplicity of 4, and each of the following columns of states (only m-values are quoted whenever there is a clearly specified j under discussion)

$$\begin{pmatrix} |\ 7/2> \\ |\text{-}7/2> \end{pmatrix} \quad \begin{pmatrix} |\text{-}5/2> \\ |\ 5/2> \end{pmatrix} \quad \begin{pmatrix} |\ 3/2> \\ |\text{-}3/2> \end{pmatrix} \quad \begin{pmatrix} |\text{-}1/2> \\ |\ 1/2> \end{pmatrix}, \tag{5}$$

transforms according to Γ_5 of D_2 in an identical manner. This means that an interaction invariant under D_2-group operations may mix up states on top of each of the above four columns. The corresponding states at the bottom will be mixed exactly in the same way as those on the top. Thus the degeneracies of the Kramer's doublets are preserved.

The ground state doublet will consist of some

$$\left.\begin{aligned} &C_7|\ 7/2> + C_3|3/2> + C_{-1}|\text{-}1/2> + C_{-5}|\text{-}5/2>, \\ &\text{degenerate with} \\ &C_7|\text{-}7/2> + C_3|\text{-}3/2> + C_{-1}|{+}1/2> + C_{-5}|\ 5/2>. \end{aligned}\right\} \tag{6}$$

An external magnetic field will split up the Kramer's doublets.[13] This is due to the last term in the Hamiltonian (1). As is well known, the information that one deduces from this kind of splitting, about the doublet structure, is essentially contained in three quantities, g_x, g_y, g_z, given by

$$g_k = \left\{1 + \frac{j(j+1) + s(s+1) - \ell(\ell+1)}{2j(j+1)}\right\} \quad \left\{J_k\right\}, \tag{7}$$

where the subscript k stands for x, y, or z, and $\{J_k\}$ is the magnitude of the difference between the eigenvalues of the two-dimensional matrix formed by the operator J_k in between the doublet states.

Experimentally, these values for Yb^{3+} : YAG are

$$g_x = 3.87,\ g_y = 3.78,\ g_z = 2.47. \tag{8}$$

Koster and Satz pointed out that a good fit to the observed g-values is given by

$$\begin{aligned} C_7 &= C_{-1} = 0 \\ C_3 &= -0.60 \\ C_{-5} &= -0.80. \end{aligned} \tag{9}$$

The g values calculated from these are $g_x = g_y = 3.80$, $g_z = 2.42$. It was first noted by Van Vleck[14] that the average of the g's of Eq. is close to the isotropic g-values found for the states (in $j = 7/2$) transforming according to the Γ_7 irreducible representation of the cubic group. This and other considerations involving the observed transitions[15] led to the hypothesis that although the actual ground state doublet belongs to the Γ_5 representation of D_2 group, it is pretty close to the doublet structure belonging to the Γ_7 irreducible representation of the cubic group (multiplicity 1 for $j = 7/2$). For this latter case

$$\begin{aligned} C_{-1} &= C_{+7} = 0 \\ C_3 &= -0.5 \\ C_{-5} &= -0.85. \end{aligned} \tag{10}$$

Koster and Satz mention the large overlap of (9) and (10) in their support of (9).

At any rate, we have accepted (9) for the ground state. In the next section we shall see that it is the simple structure of (9) that greatly facilitates the problem of correlating the energy matrix elements to the observed eigenvalues in $j = 7/2$ space.

SEARCH FOR A SELF CONSISTENT SOLUTION

With the ground state decided upon, we write down in full generality the wave functions for $j = 7/2$ manifold:

m	(I)	(II)	(III)	(IV)	
7/2	0	A	B	C	
3/2	-0.6	0.8x	0.8y	0.8z	(11)
-1/2	0	a	b	c	
-5/2	-0.8	-0.6x	-0.6y	-0.6z	

II, III, and IV are each orthogonal to I.
Orthogonality relations among them are:

$$AB + xy + ab = 0 \tag{12}$$
$$BC + yz + bc = 0 \tag{13}$$
$$CA + zx + ca = 0 \tag{14}$$

Let us assume that none of the nine coefficients is zero. Then, dividing (1), (2), and (3) by AB, BC, and CA, respectively, and denoting x/A by x' and a/A by a', etc., we get

$$1 + x'y' + a'b' = 0 \tag{12a}$$
$$1 + y'z' + b'c' = 0 \tag{13a}$$
$$1 + z'x' + e'a' = 0. \tag{14a}$$

From (12a) we have

$$y' = -\frac{1 + a'b'}{x'};$$

and from (14a).

$$z' = -\frac{1 + c'a'}{x'}.$$

Then, from (13a)

$$\frac{(1 + a'b')\ (1 + c'a')}{x'^2} + (1 + b'c') = 0;$$

therefore,

$$x' = \pm\left(\frac{(1 + a'b')\ (1 + c'a')}{(1 + b'c')}\right)^{1/2}. \qquad (15)$$

Therefore, from (1b) we have

$$y' = \pm\left(\frac{-(1 + a'b')\ (1 + b'c')}{(1 + c'a')}\right)^{1/2}\ ; \qquad (16)$$

and from (3b)

$$z' = \pm\left(\frac{-(1 + c'a')\ (1 + b'c')}{(1 + a'b')}\right)^{1/2}. \qquad (17)$$

But, putting these values of y' and z' in (2a), one gets

$$(1 + b'c') + (1 + b'c') = 0$$

or

$$1 + b'c' = 0,$$

which means that either y' or z', or both, are equal to zero, contradicting the assumption that none are equal to zero. Thus we conclude that at least one of the nine coefficients is equal to zero.

A typical case is illustrated below. Choose A equals zero in (11). Then

$$\left.\begin{aligned} xy + ab = 0 \quad &\longrightarrow \quad y = -\frac{ab}{x} \\ zx + ca = 0 \quad &\longrightarrow \quad z = -\frac{ca}{x} \end{aligned}\right\} \quad \text{provided } x \neq 0 \qquad (18)$$

$$Bc + yz + bc = 0.$$

The last identity becomes

$$BC + \frac{a^2bc}{x^2} + bc = 0;$$

and if b and c are not equal to zero, we get

$$1 + \frac{a^2}{x^2} + B''c'' = 0,$$

where $B'' = B/b$ and $c'' = C/c$. Thus if A equal zero and x, b, and c do not equal zero, we can write the wave function as

$$\begin{matrix} \text{II} \\ \begin{pmatrix} 0 \\ 0.8 \\ a/x = a'' \\ -0.6 \end{pmatrix} \end{matrix} \quad \begin{matrix} \text{III} \\ \begin{pmatrix} B'' \\ 0.8y'' \equiv 0.8\ y/b \\ 1 \\ -0.6y'' \end{pmatrix} \end{matrix} \quad \begin{matrix} \text{IV} \\ \begin{pmatrix} C'' \\ 0.8z'' = 0.8\ z/c \\ 1 \\ -0.6z'' \end{pmatrix} \end{matrix} \qquad (19)$$

with $1 + a''^2 + B''\ C'' = 0$.

Let E_1, E_2, and E_3 be the eigenvalues of the eigenvectors (II), (III), and (IV), respectively, and let V denote the secular matrix in the $j = 7/2$ space. Applying V on each of these wave functions, one is most generally able to express each matrix element as a function of E_1, E_2, E_3, B'', C'', a'', y'', z''

$$V_{ik} = V_{ik}\ (E_1,\ E_2,\ E_3,\ B'',\ C'',\ a'',\ y'',\ z''). \qquad (20)$$

Actually, in this case, a'', y'', and z'' can be eliminated, and one finally will obtain

$$V_{ik} = V_{ik}\ (E_1,\ E_2,\ E_3,\ B'',\ C''). \qquad (20a)$$

Now there are six ways in which one can associate E_1, E_2, and E_3 with the three experimental values. We can thus construct, even for (8), six distinct secular matrices, each with two floating parameters. For any values of these two parameters, each will reproduce the experimental energy values. The idea now is to pick those which for some values of B'', C'' will reproduce the observed energy levels for $j = 5/2$ manifold. The calculation now is through standard Racah algebra. For a general V-matrix, the parameters a_q^k coming in $H_{crystal}$ in (2) can be calculated in terms of V_{ik}'s. Let W denote the 3 x 3 energy matrix of the $j = 5/2$ manifold. Then, the matrix elements W_{ik}'s can also be expressed in terms of V_{ik}'s. The procedure is schematically as follows.

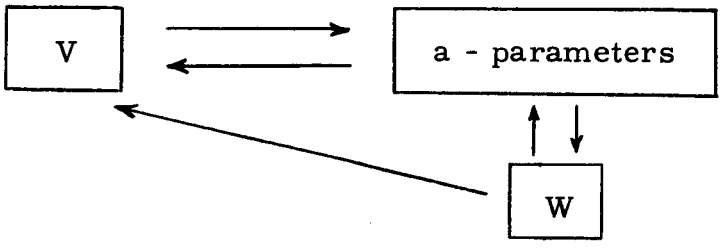

Picking a particular possibility for the V-matrix (i. e., every association of E_1, E_2, and E_3 with observed values), we have a unique set of expression for W_{ik}'s,

$$W_{ik} = W_{ik} \ (E_1, E_2, E_3, B'', C''). \tag{21}$$

The solutions of the equation

$$\det \left| W - \lambda \delta_{ik} \right| = 0 \tag{22}$$

are the eigenvalues of the W-matrix. This equation is cubic in λ with B'' and C'' entering non-linearly in the coefficient of λ and in the term free of λ. Since the V-matrix is traceless, so is the W-matrix. If W_1, W_2, and W_3 are the three observed levels in $j = 5/2$ manifold, measured from the center of gravity of the spectrum, then the left-hand side of (21) should be identically equal to

$$\begin{aligned} &(W_1 - \lambda)\ (W_2 - \lambda)\ (W_3 - \lambda) \\ &\equiv -\lambda^3 + \lambda\ (W_1^2 - W_2 W_3) + W_1 W_2 W_3. \end{aligned} \tag{23}$$

It is a simple matter to check whether any set (or sets) of values of B'' and C'' can satisfy the equality. This has to be done for all modes of simflification (12 - 14) are for every association of (E_1, E_2, E_3) with observed values in a given mode.

For the sake of completness of this one case, we note that, if in (18)
$x = 0$, then
$ab = 0$
$ca = 0$.

Therefore, either $a = 0$, in which case wave function II is null, which is absurd, or $b = 0$, $c = 0$

(24)

Then $BC + yz = 0$.

One can proceed with this case, viz $A = 0$, $x = 0$, $b = 0$. $c = 0$ to seek compatibility of (22) with (23). Other major cases start out assuming $x = 0$ (i. e., one amplitude in the second and fourth row of any one of the state vectors becomes zero) and $a = 0$.

EXPERIMENTS

MICROWAVE RESONANCE OF METASTABLE STATES

Some preliminary steps were taken at the beginning of the contract period toward construction of a microwave spectrometer for time resolved studies of microwave absorption by metastable paramagnetic levels in crystals. The initial aim was to observe the microwave resonance of the metastable $^4F_{3/2}$ levels of Nd^{3+} in YAG, as well as the ^2E levels of Cr^{3+} in YAG using available laser rods. Optical spectroscopic studies, including measurement of Zeeman effect in laser emission from these materials, were made under a previous contract.[1] Microwave absorption by the ^2E states of Cr^{3+} in ruby has been observed by Geschwind, et al.[2], and microwave absorption from the paramagnetic triplet states of aromatic molecules has been extensively studied since the pioneering experiments of Hutchison and Mangum.[3] These techniques do not seem to have been extended to the study of other inorganic ions in crystals, probably because of the experimental problems involved. It seems that the utilization of optical pumping techniques developed for laser pumping along with pulsed microwave techniques utilizing signal averaging over repetitive pulses should permit study of a variety of such systems.

For the purpose of obtaining detailed energy level assignments in a rare earth ion spectrum such as Nd^{3+}, magnetic field splitting of the otherwise degenerate Kramer's doublets is a considerable help. The optical lines, however, are broadened by the interaction of the latice vibrations with the local field in the vicinity of the ionic sites (thermal broadening) and random perturbations of the local field by lattice imperfections (strain broadening). The optical spectra of Nd^{3+} in YAG are therefore limited in resolution to approximately 0.5 cm^{-1} at 10,000 cm^{-1}, or 5 parts in 10^5. If we assume that the local field dependence of the microwave transition energies is of the same order as the optical transition energies (which is roughly correct for ground state spectroscopy), then at 10 GHz we would be able to resolve shifts of the order of 1 MHz, or about 3×10^{-4} cm^{-1}, thus obtaining much more accurate "g" values than is possible optically. Aside from this higher resolution, independent measurements of decay rates and degree of depletion of ground state population during optical pumping could be obtained by such measurements. Such measurements made during laser oscillation would be particularily interesting.

Figure 3 shows a block diagram of the proposed spectrometer. The microwave spectrometer is conventional aside from the use of a pulsed source and time resolved detector. The pulsed source is used in the hope

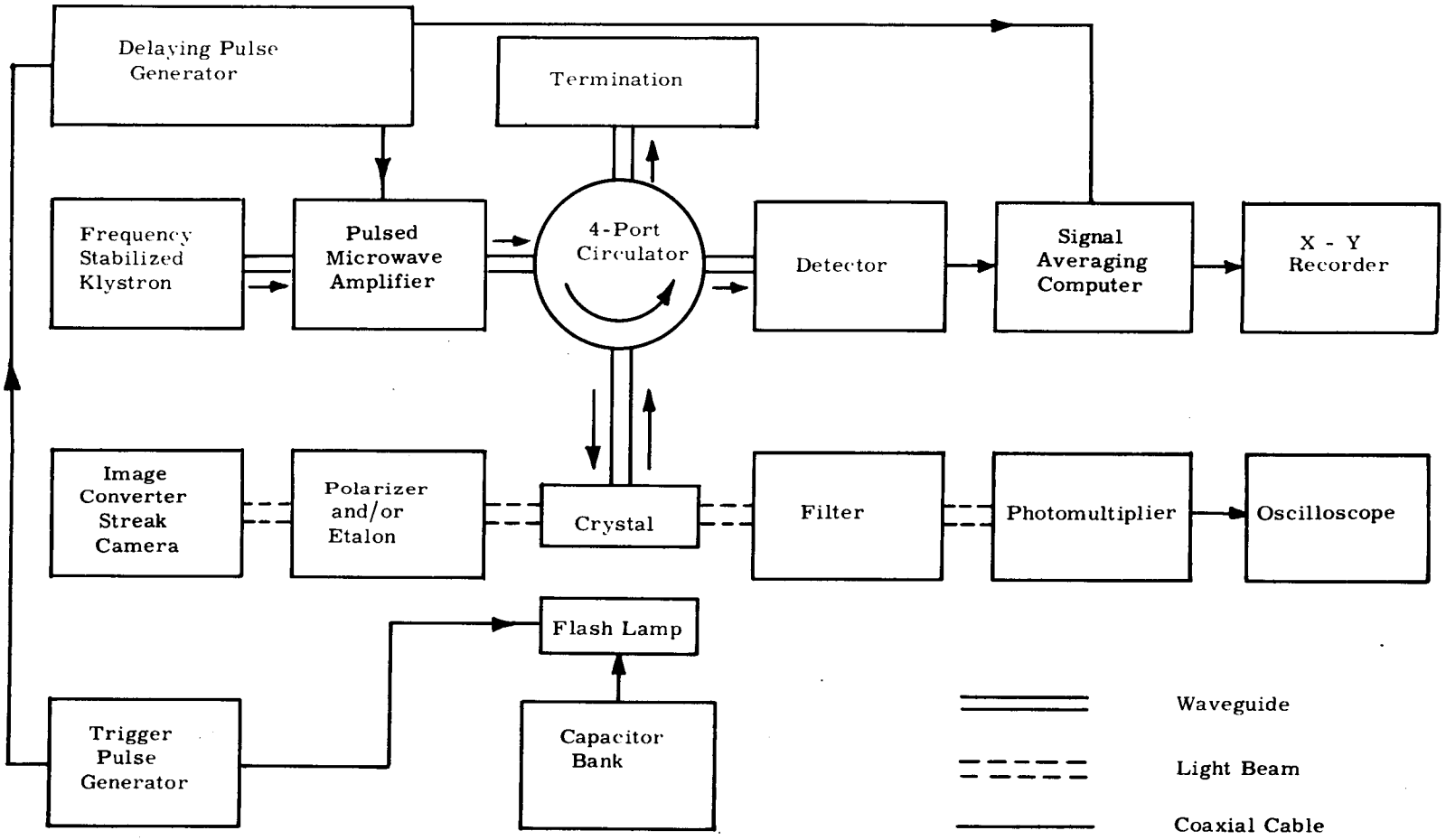

Fig. 3. Block diagram of proposed microwave spectrometer.

that higher power levels might be tolerated without saturation on a pulsed basis. Whether or not this is so depends on the spin-lattice relaxation time for each experimental situation, and cannot be predicted a priori. The results of Scott and Jeffries[23] seem to indicate very rapid spin lattice relaxation in Nd^{3+} above 10°K, although YAG matrix was not measured by them. The streak camera is intended to permit observation of the time and angle dependence of the laser output, in cases where the sample is being operated as a laser. The photomultiplier permits observation of laser intensity and fluorescent decay time. The fluorescent decay can also be averaged over a series of pulses to permit comparison with the decay of the microwave resonance.

The sample holder labeled "crystal" in Fig. 3 is shown in more detail in Fig. 4. The pump reflector is similar to that used for the transverse Zeeman effect study of Ref. 1, so that it can be inserted into the 2-1/2 in. pole gap of a 12-in. electromagnet. Windows are provided at both ends of the holder so that the sample rod can be either coated with reflectors on its end surfaces or used with external mirrors. The sample rod is used as a dielectric cavity, the microwave frequency being chosen to coincide with a sample rod length resonance when it is excited in the TE_{11n} mode. Although the microwave field extends into the space surrounding the rod to some extent, the field at the flash lamp was calculated to be very small when the rod diameter is close to a half wavelength of the microwave radiation within the rod. Since this cavity was never tested, the degree to which interaction with the pump lamp can be avoided is uncertain. If the pump pulse can be made much shorter than the metastable life time, the microwave pulse can be delayed until after the pump lamp plasma is extinguished, thereby avoiding the residual microwave absorption effect of the plasma.

For the case of Nd^{3+} in YAG, a further alternative exists. It has been shown that Nd^{3+} can be pumped by a ruby laser by using the edge of the $^4F_{9/2}$ absorption band. Use of a Q-spoiled ruby laser, therefore, would permit pumping along the axis of the rod without requiring the pump lamp or reflector. This would certainly make for a "cleaner" experiment although care must be taken to avoid power levels which would damage the YAG rod.

The construction and operation of a microwave-optical spectrometer of the type outlined above would have required considerable additional capital equipment investment and would have required most of the current contract period simply to place it in operation. When it was learned that long-term continued effort along these lines was improbable, discussions with the contract monitor resulted in agreement to discontinue this aspect of the contract work and concentrate on the theoretical work and optical spectroscopy.

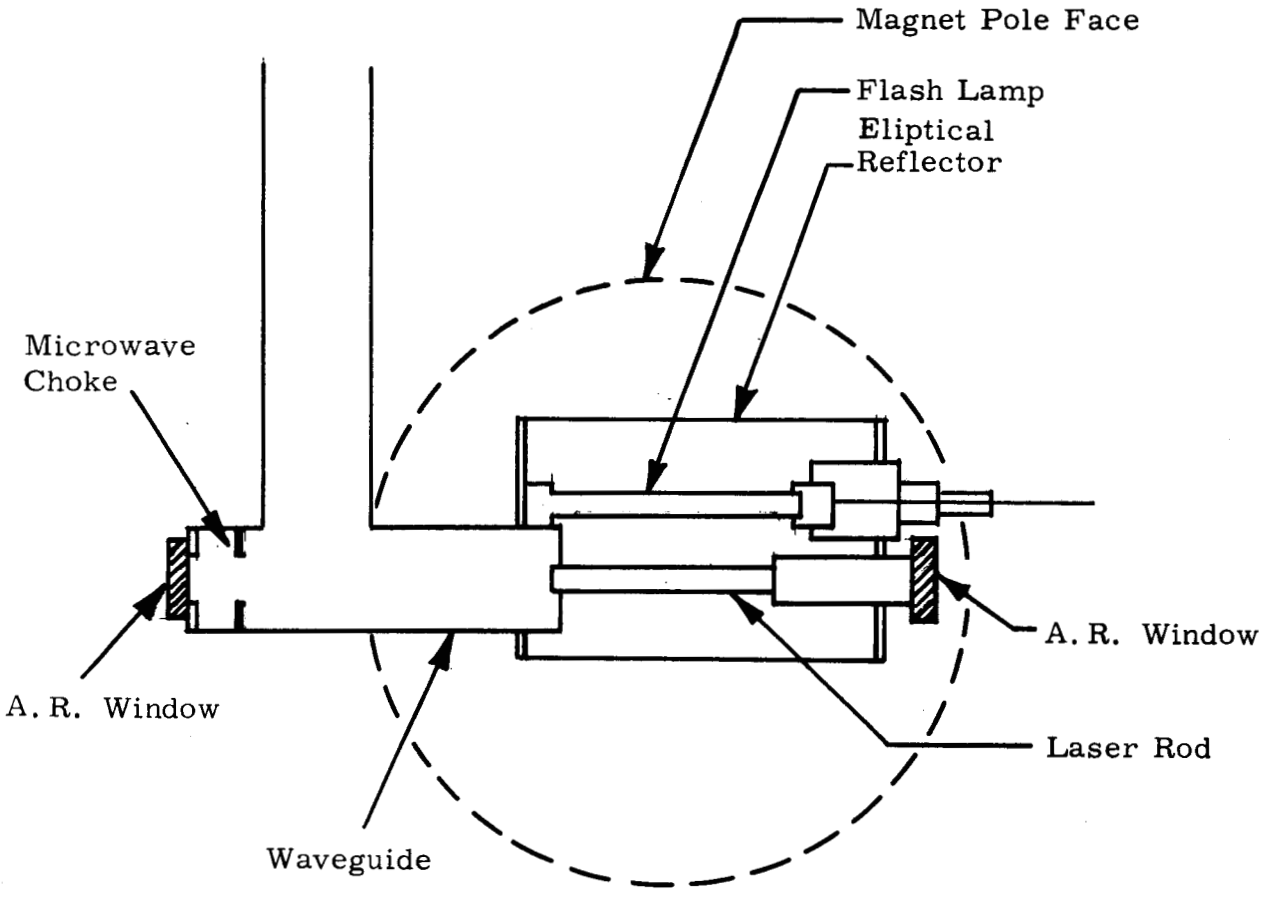

Fig. 4. Schematic diagram of sample mounting in magnet pole gap.

METASTABLE STATE OPTICAL ABSORPTION

Development of Scanning Spectrometer for Metastable State Absorption Spectroscopy

Optical absorption by metastable states can have a marked influence on the efficiency of optically pumped laser materials, as discussed in Ref. 5 and in the preceding section "Metastable State Absorption." The determination of the extent to which such absorption influences the operation of Nd^{3+}: YAG lasers is the object of the measurements to be presented here.

Since the optical absorption spectrum of Nd^{3+}: YAG consists of many fairly narrow lines, rather than fairly broad bands as in ruby, it was essential to build an automatic scanning spectrometer of moderate resolution in order to obtain the data at a reasonable rate. A block diagram of the spectrometer system is shown in Fig. 5. The system consists of three parts whose operation is coordinated by a clock circuit. The three subsystems, which are described in detail below, are (a) the probe lamp, (b) the sample and pumping head, and (c) the monochromator-detector. Before describing the sub-systems, we will outline the operation of the spectrometer.

The xenon arc lamp, acting as a pulsed "white" light source, is triggered about once every 5 sec. The light passes through the sample, which is alternatly pumped and unpumped, and through the monochromator which transmits only a narrow wavelength band to the detector. The detector is gated in synchronism with the probe pulse to minimize pickup of stray pump light and fluorescence. The current pulse from the detector is integrated, and the integrated pulse intensity is then displayed on a chart recorder. The integrator is discharged before the next probe pulse, and the monochromator pass band is scanned slowly to yield an output of alternate unpumped and pumped transmission as a function of wavelength. A scan also is made without the sample to obtain the spectrum of the initial intensity of the probe lamp.

Clock Circuits. - The pulse timing circuits are shown in Fig. 6. The basic clock circuit consists of a pair of time delay relays which can be adjusted to give probe pulse intervals from 1.8 sec to 180 sec. The master clock pulse for the pump, probe, and detector circuits is generated by the breaking of contacts 1 and 4 of Relay 2, which interrupts the battery circuit for about 50 msec at the beginning of each cycle. The break provides a clean pulse of reproducible timing, but subsequent contact bounce generates

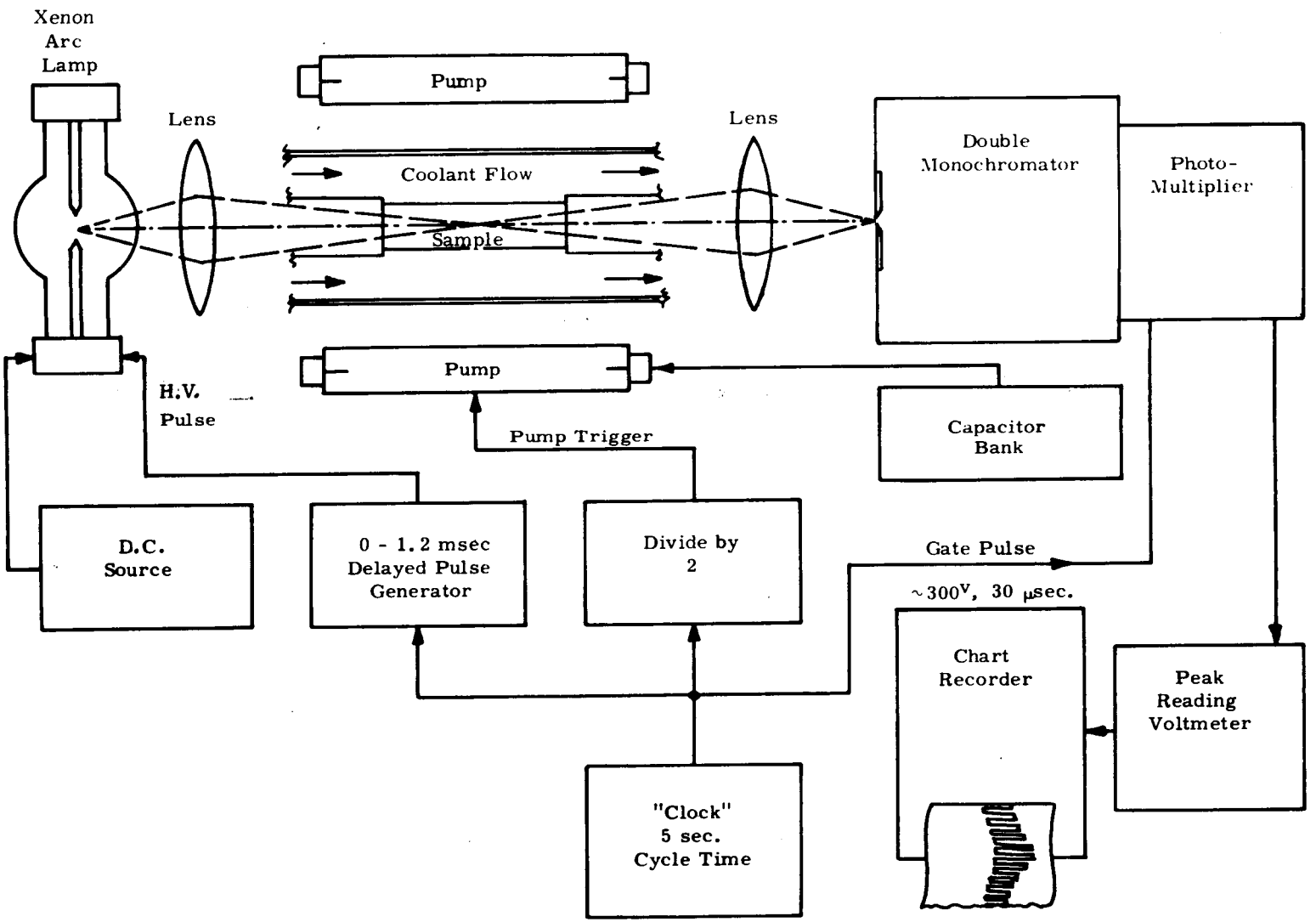

Fig. 5. Block diagram of metastable state absorption spectrometer.

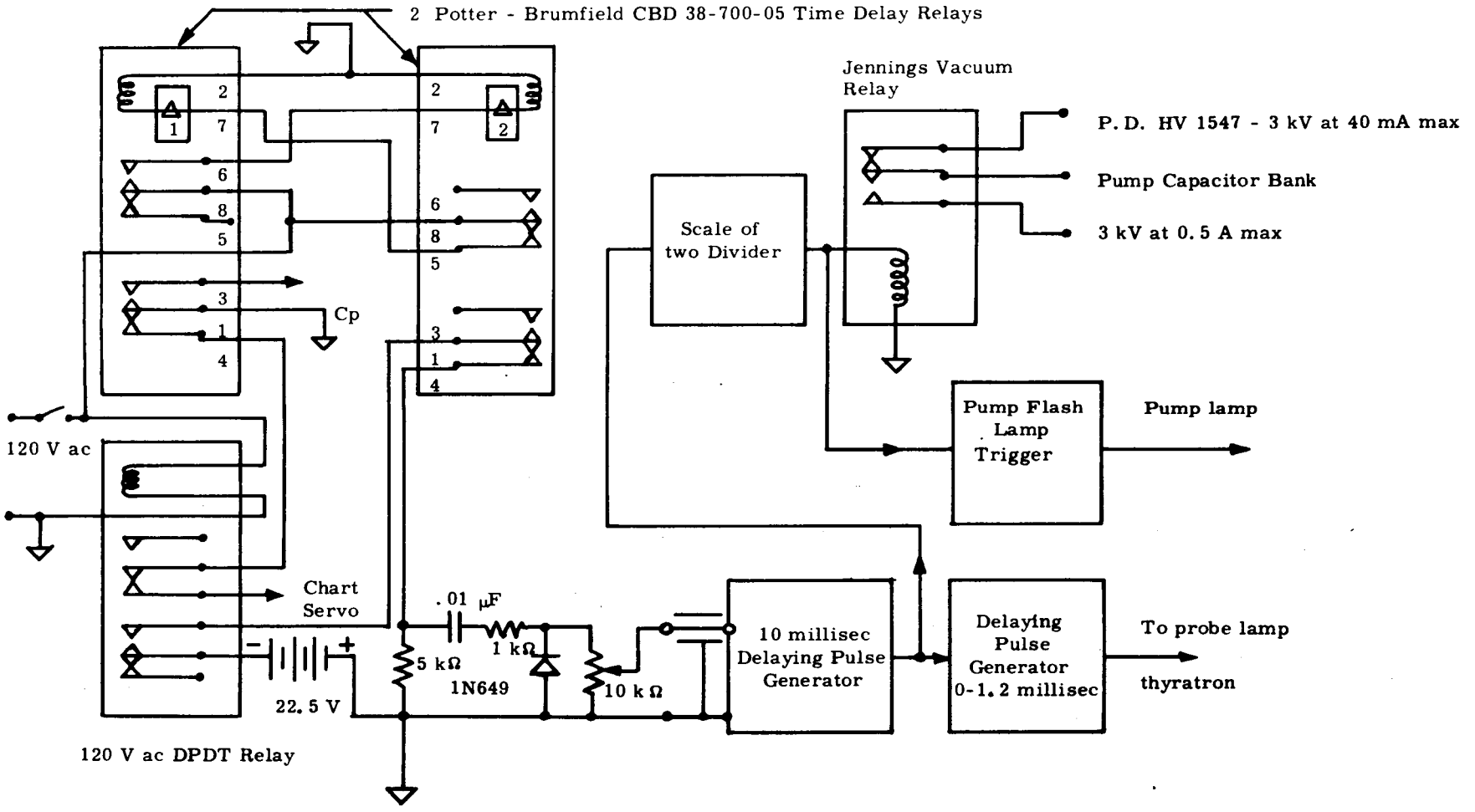

Fig. 6. Schematic diagram of pulse timing circuits.

spurious pulses which are removed by buffering the master pulse with a 100-msec delay generator, during which delay no other pulses can pass through. The delayed master pulse then triggers both the scale of 2 divider, which triggers the pump lamp on alternate clock pulses, and the probe and detector delay generator. The delay of the probe behind the pump trigger can be adjusted from -2 μsec to 1.2 msec. This delay range proved adequate for Nd: YAG, although longer delays might be desirable for other materials. The delayed pulse then triggers the probe lamp and detector gate amplifier. The clock relay also discharges the peak voltmeter capacitor before the next probe pulse, and disables the chart recorder pen servo during the capacitor discharge to avoid excessive pen motion. The pulse width of the delayed pulse can be varied to optimize rejection of light signals (e.g., scattered pump light or fluorescence) having a longer period than that of the probe pulse. The timing of the various circuits is shown in Fig. 7.

Probe pulse circuits. - The lamp used to generate the probe pulse is a PEK Lab's X-80 compact xenon arc lamp. This lamp has heavier leads than standard compact arc lamps to improve its pulsed current handling ability. When operated as a continuous lamp, the X-80 provides stable operation with 3 to 5 A dc at about 14 V drop across the lamp. The bright region of the arc is about 0.3 mm in diameter located near the cathode in this mode of operation, and has some tendency toward random displacements perpendicular to the electrode axis about equal to its diameter. When the lamp is operated with a high-voltage pulse superposed on the dc excitation, the arc volume increases to about 1 mm diameter, centered between the electrodes, but it is very stable in position. For optimum use of pulsed light output, the optical system should be designed to utilize the 1-mm diameter source rather than the smaller and somewhat displaced dc arc source. We have found pulse energy inputs of about 1 J to be consistent with reasonable lamp life (about 10,000 flashes). Optimum voltage depends on the wavelength region in which operation is desired. Ultraviolet operation seems best with high voltage (up to 10 kV has been used in our laboratory), whereas near infrared operation requires relatively low voltage (about 500 V). Afterglow seems to limit pulse duration to greater than 5 μsec between the one-third peak intensity points, even when the current pulse is sub-microsecond. In the experiments presented below, pulse durations of about 15 μsec were used since Nd: YAG decay time of about 200 μsec did not require shorter pulse durations.

The probe pulse and dc arc circuits are shown in Fig. 8. The hydrogen thyratron-ignitron combination is greatly overdesigned for this application since it was designed to handle about 500-J pulses at 10 kV.

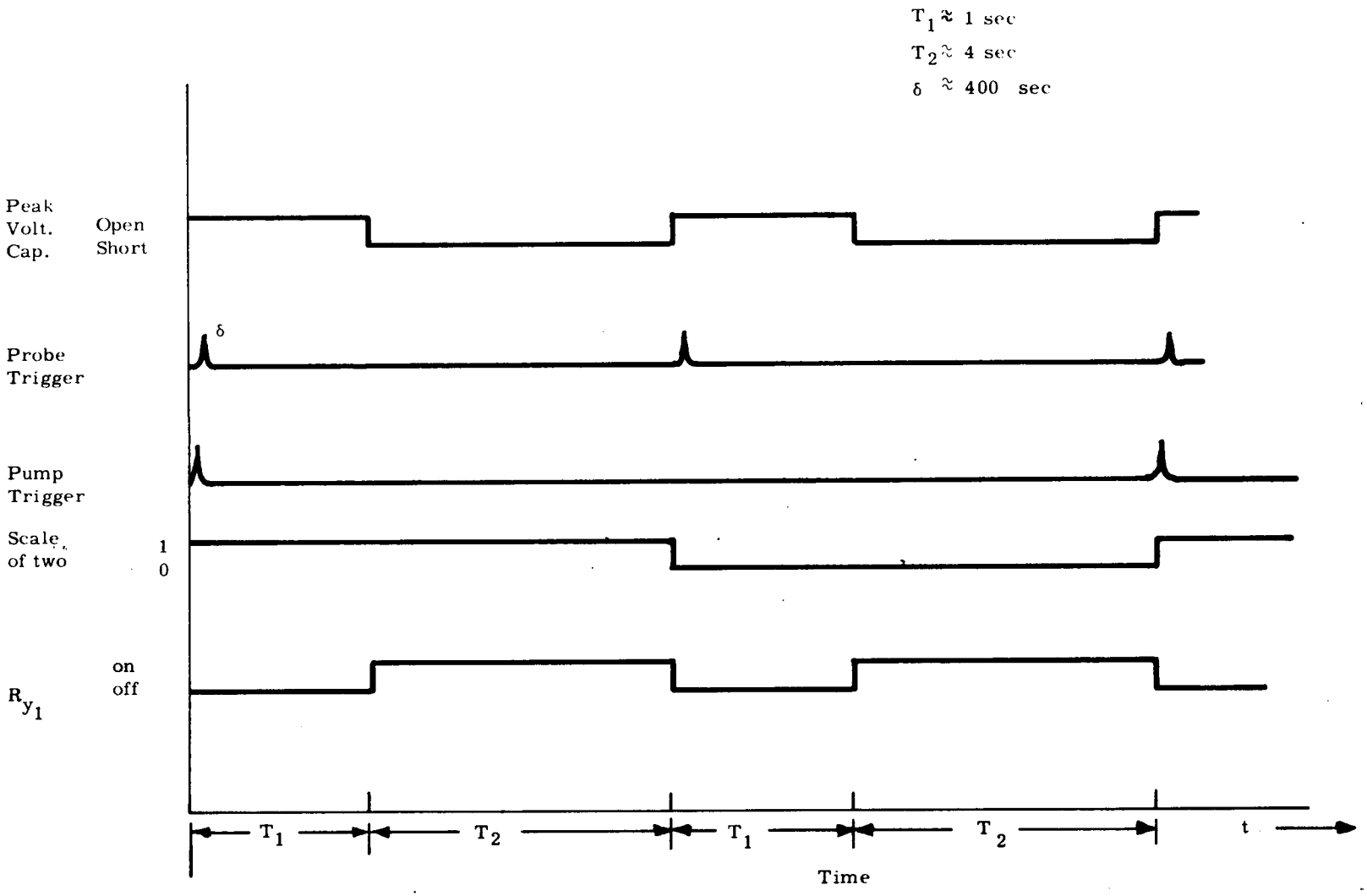

Fig. 7. Timing sequence diagram.

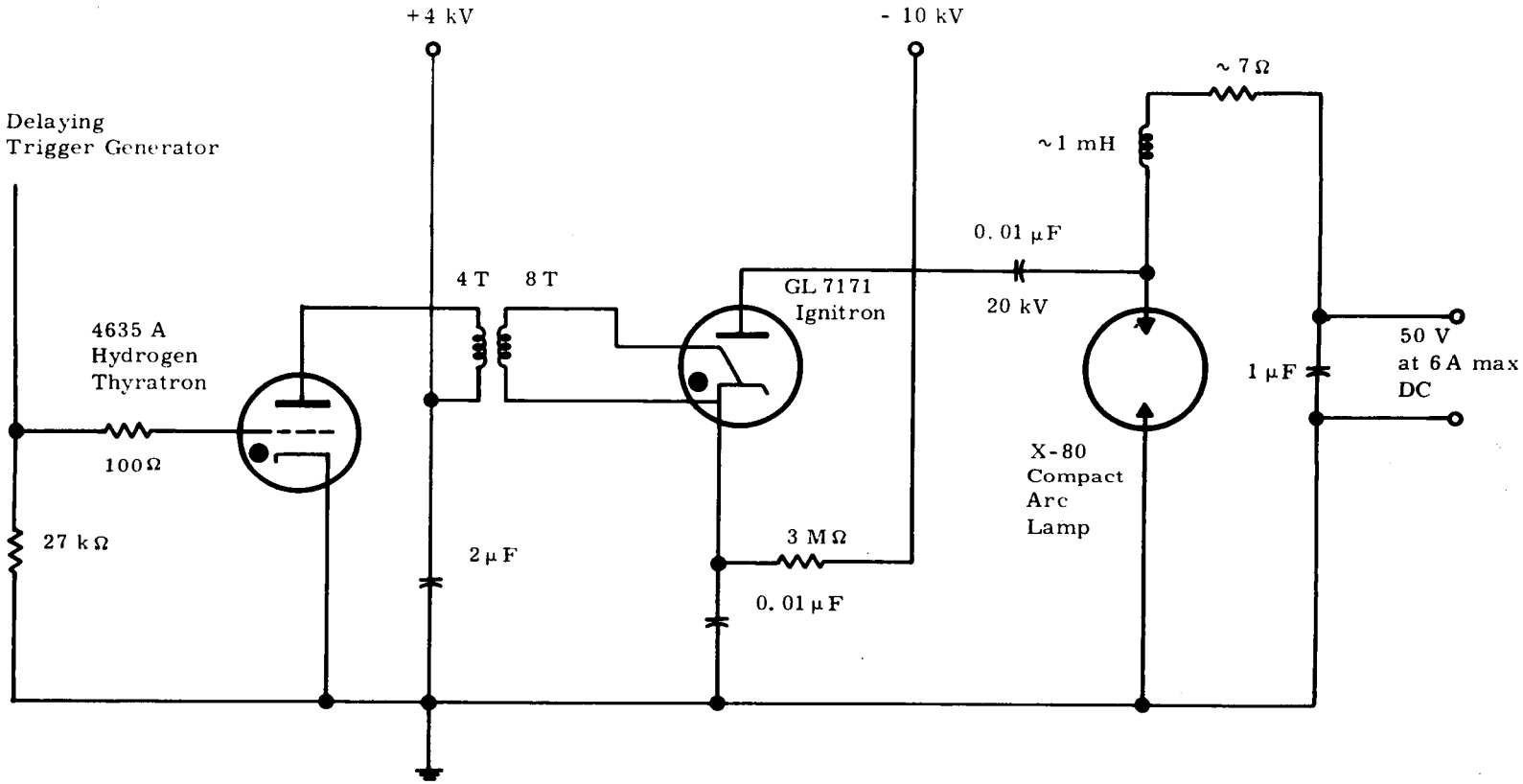

Fig. 8. Probe lamp circuits.

The equipment was available from another experimental setup. Since this equipment worked very well, no modifications were made. If the high-voltage switching ignitron had not been available, the thyratron alone could easily have been used to handle the probe pulse requirements. The large air core inductor was used as a ballast rather than the purely resistive ballast usually used with these lamps in order to provide a higher impedance to the short pulse.

Sample and optical pump. - The optical pumping arrangement was designed to accommodate crystals up to 2 in. long and 1/4 in. o.d. It uses a double elliptical cylinder reflector. This reflector has fairly high efficiency and minimal length for fairly large aperture light transmission through the sample. Cross sections of the optical pumping arrangement are shown in Fig. 9. The gold plated copper reflector was chosen for pumping into the near infrared absorption bands of Nd^{3+}: YAG. Uniformity of pumping is fairly important in this instrument since thermal stresses due to uneven pumping cause distortion of the crystal and attendant changes in transmitted beam geometry. Because of the limited monochromator slit acceptance of the incident beam, changes in beam position result in changes in transmitted intensity upon pumping which can only be resolved from true metastable state effects by a study of their time dependence. A single ellipse introduced considerable wedge error into the sample, with attendant beam deflection, whereas a negligible effect has been noted with the double ellipse arrangement.

The pump lamps are two PEK Lab's XE1-2 linear flashlamps, operated in series and triggered in parallel. The pump circuits are shown in Fig. 10. The end triggering is convenient since it avoids the requirement of adequate clearance between flashlamp and reflector housing to avoid arcing from the trigger wire to the reflector. The resistor-inductor network is required because the first flashlamp to break down under the trigger pulse tends to load down the trigger circuit so much that there is insufficient voltage to trigger the other lamp. This either/or operation is avoided by inserting a pair of series resistors to set the minimum trigger output load. The inductor carries the main discharge current but provides some isolation between the lamps with respect to the trigger voltage.

In order to pump at fairly high repetition rates, but maintain reproducible pulses, two capacitor bank charging supplies are used. One is capable of supplying 0.5 A at up to 3 kV. This supply is used to provide the initial charge, about 30 V below the desired final charging voltage. When the unpumped probe pulse is triggered, a vacuum relay switches out

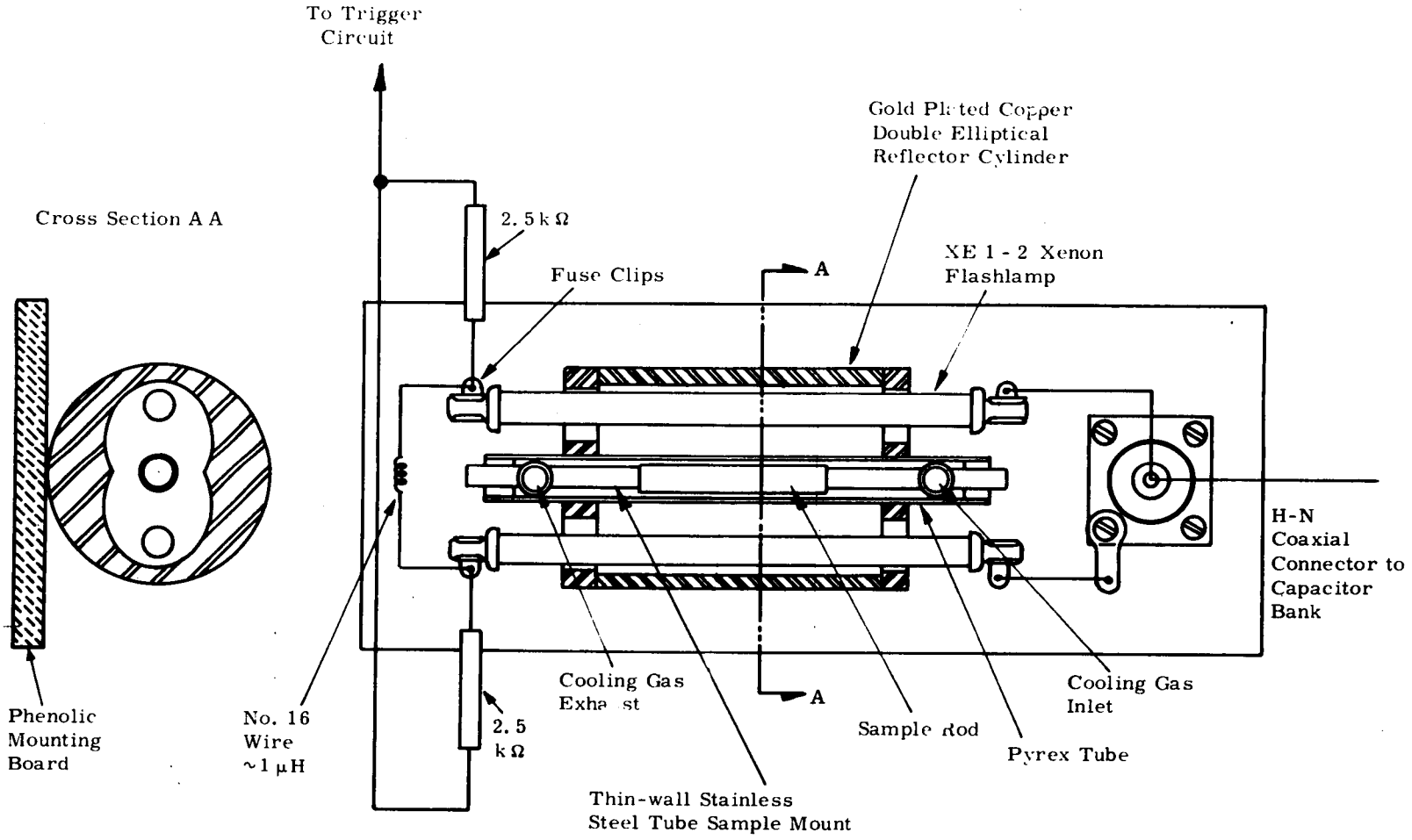

Fig. 9. Pump cavity cross section.

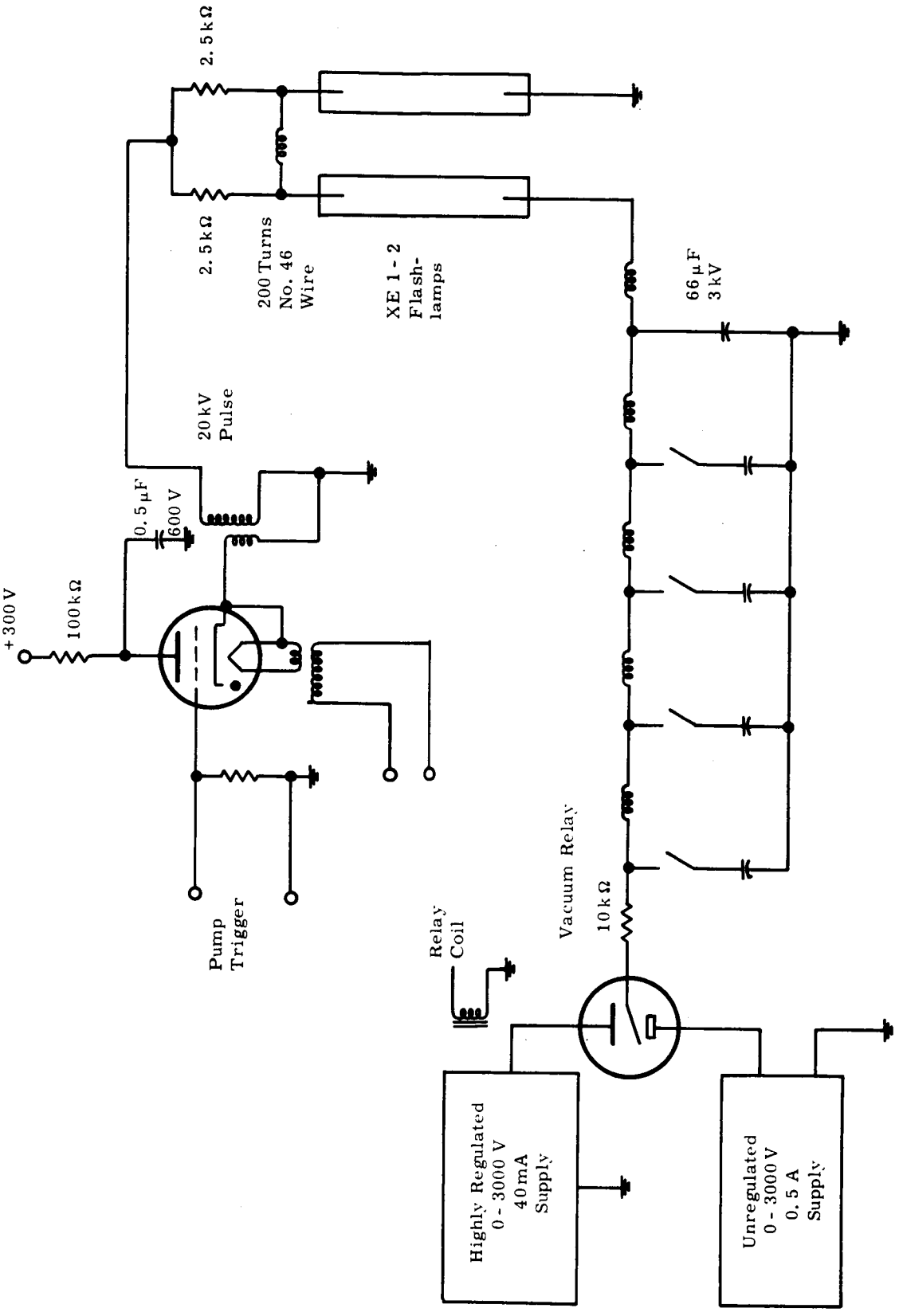

Fig. 10. Pump circuits.

the high-current supply and connects a low output impedance, highly regulated supply across the capacitor bank. The capacitors are therefore charged to within the ±0.1 percent voltage precision of the regulated supply just before the flashlamps are triggered.

The sample temperature is monitored with a thermocouple and regulated by adjusting the flow rate and temperature of cool nitrogen gas circulated past it. Sample temperature is raised a few degrees by typical pump pulses, but returns to the initial temperature before the next pump pulse under steady state conditions. The flashlamps are cooled by slow air circulation through the cavity. The repetition rate of pump pulses could be increased by at least an order of magnitude if water cooling were used.

Monochromator and detector. - Discussed below are (1) the monochromator, (2) photomultiplier and dynamic range, and (3) pulse amplification and recording.

(1) Monochromator

In selecting a monochromator for use with this spectrometer, we had to compromise between three conflicting requirements: (a) large aperture to obtain adequate flux in the short pulse for reasonable photon statistics, (b) adequate resolution for absorption lines a few angstroms wide, and (c) low transmission of scattered light outside the pass band, to permit accurate measurement of strong absorption peaks. The Jarrell-Ash Model 82-400 dual monochromator meets these requirements fairly well although some sacrifice in aperture at the expense of greater resolution might have been desirable for work with Nd^{3+}: YAG at room temperature. Resolution is limited to about 5 Å in the visible and near infrared because the quality of the optical elements (particularily the spherical mirrors) does not permit achievement of theoretical resolution. Scattered light rejection is quite good although we have found it necessary to use additional band pass limiting filters (usually colored glass filters produced by Corning Glass Works) when the optical density of the sample exceeded 2. The monochromator's wavelength drive is geared to a synchronous motor having a variable gearbox with a range of drive speeds covering a 50:1 range.

(2) Photomultiplier Gating and Dynamic Range.

Photomultiplier tubes were used for measurements between 3000 Å and 10,000 Å, an EMI 9558B having S-20 response and an Amperex 150 CVP having S-1 response, covered the required spectral range, the crossover in sensitivity coming at about 7500 Å. In order to minimize the pickup of scattered pump light and fluorescence, the photomultipliers were gated off except during the probe pulse. A technique for dynode gating was developed which proved very stable and permitted operation of the photomultiplier from a highly regulated dc supply for reproducibility of gain. The circuit is shown in Fig. 11. Only the potential of one dynode is influenced by the gate pulse so that slight pulse amplitude jitter has little influence on gain.

Tests of the gating characteristics using a continuous light source showed that as long as the gated dynode had a potential a few volts lower than the next lower dynode, or a few volts higher than the next higher dynode, no current was transmitted to the anode. When the dynode was pulsed to a potential intermediate between the two adjacent dynodes, gain rapidly approached a plateau equivalent to normal uniform field operation, as shown in Fig. 12. The overall photomultiplier gain is therefore set by the stable high voltage supply, and is insensitive to slight fluctuations in gate pulse amplitude either from pulse to pulse or with time during a single pulse.

The dynamic range of a photomultiplier used with short pulses of light is limited at low intensity by photoelectron counting noise enhanced by multiplier gain variations. In some cases (S-1 surface at room temperature) shot noise due to dark current sets the minimum detectable level. At high intensities either dynode saturation or photocathode saturation limits the anode current. Dynode saturation can be avoided by using low impedance resistor dividers with capacitative bypass having a time constant long compared with the pulse duration, and by keeping the gain low enough to avoid exceeding the peak current ratings of the tube. Cathode saturation in end window photocathodes is a result of the high resistivity of the photocathode and its substrate, which permits positive charge build up during high intensity light pulses. The two different sources of saturation

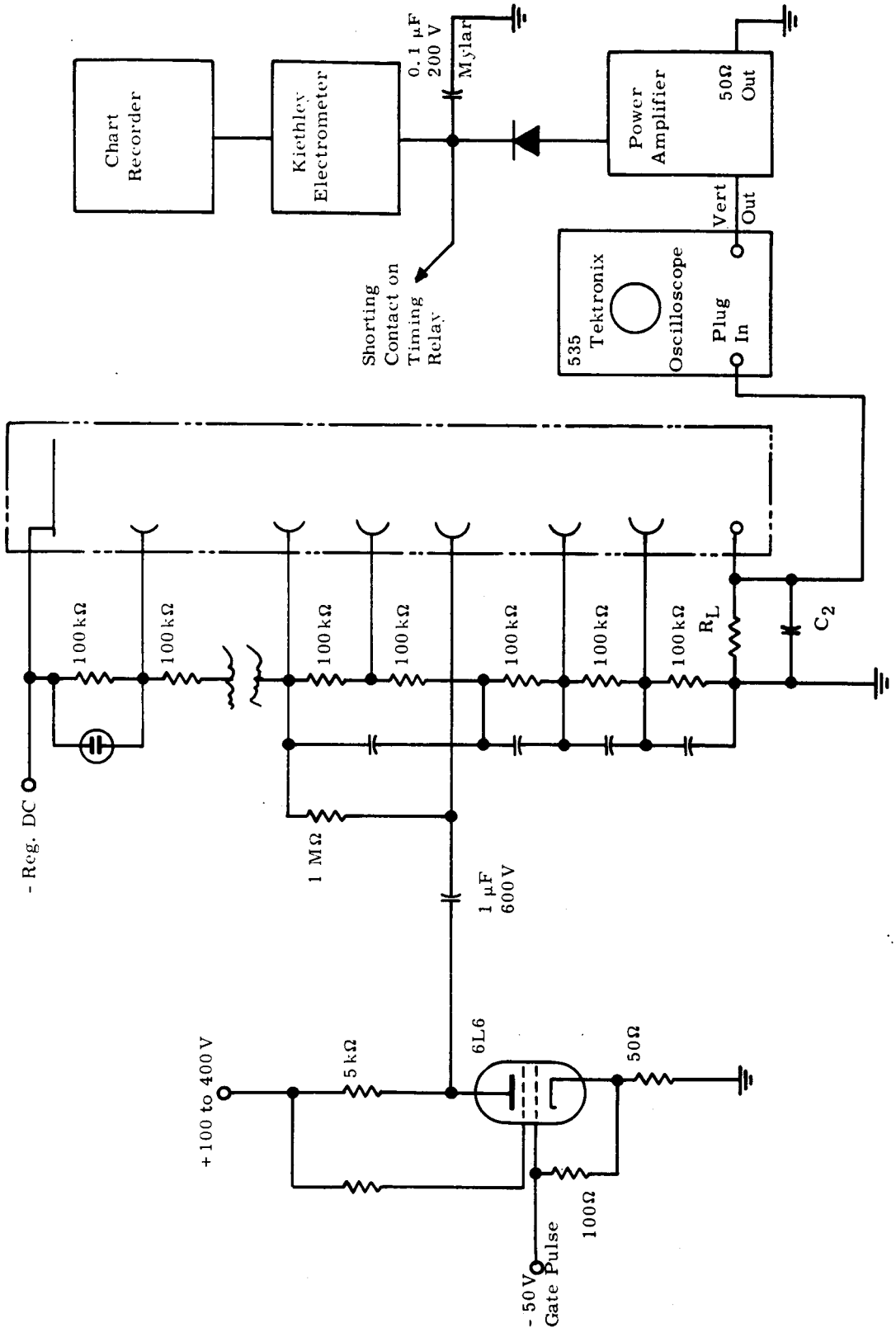

Fig. 11. Detector circuits.

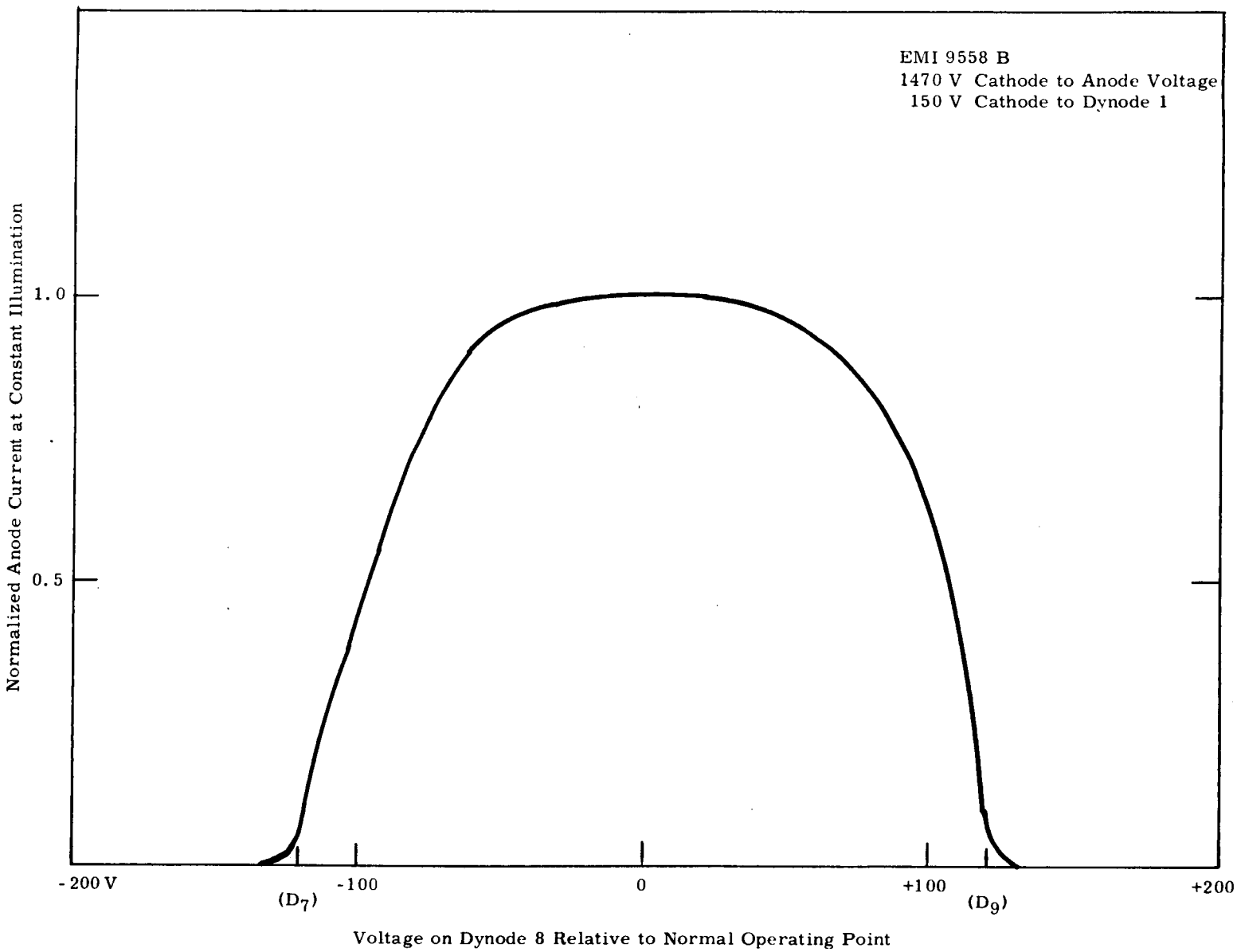

Fig. 12. Anode current as function of variable potential on one dynode of multiplier chain.

can be distinguished by observing the saturation as a function of multiplier gain. Dynode saturation results in saturation at a fixed anode current, independent of changes in gain, whereas cathode saturation occurs at the same light intensity independent of multiplier gain. A typical saturation curve for a 9558 B operated near the high gain end of the cathode saturation region is shown in Fig. 13. The measurements are taken using "neutral density" filters calibrated in the same apparatus and wavelength band at lower light intensity. The saturation measurements with 15-μsec pulses were very reproducible, so that the low duty cycle overloading of the tube does not appear to damage it. In actual measurements we avoided operation in the region where more than a 5 percent correction of the output current was required. Because of the statistical fluctuations due to the finite number of photoelectrons per pulse, it is desirable to operate as close to saturation as possible. If higher brightness probe sources are used (e.g., lasers), metal substrate photocathodes would be required for optimum signal-to-noise ratio.

(3) Pulse Amplification and Recording.

The anode pulse is integrated and amplified by an oscilloscope amplifier. The amplifier gain is adjusted to maintain output readings between 90 percent and 20 percent of full scale. The oscilloscope's vertical output is amplified by a linear amplifier with an output impedance of about 50Ω and capable of generating 100 V peak across its output. The peak voltage out of the linear amplifier is proportional to the integrated photomultiplier anode current during the gate pulse. The capacitor C_p is charged to the peak voltage through diode IN649. The diode has a very high back resistance when reverse biased by 10 to 100 V, so the time constant for discharge of the capacitor is several minutes. The Keithley 210 electrometer input impedance of 10^{10} ohms does not appreciably decrease the time constant of this circuit. Since the chart recorder, which is connected to the electrometer output terminals, has a full-scale response time of about 1 sec, the time constant of the peak voltmeter circuit is adequate for permitting chart recorder readout without drop off. Some non-linearity is inherent in this method of reading peak voltages because of the highly non-linear diode forward resistance during the charging of the capacitor. In order to permit readings to the one-quarter percent full-scale accuracy of the chart recorder,

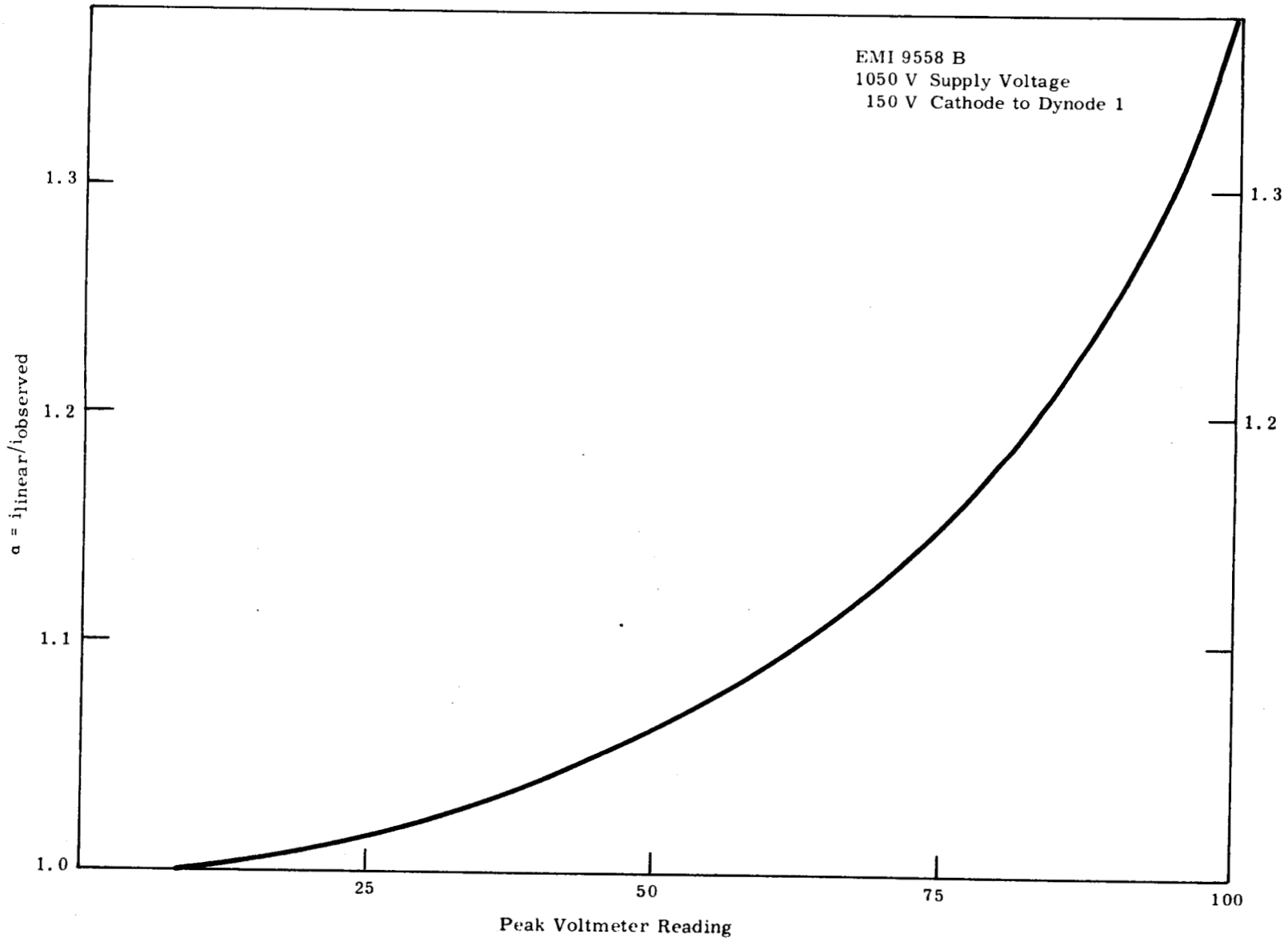

Fig. 13. Photomultiplier saturation characteristic in cathode saturation domain.

we plotted a calibration curve using a pulse generator with a precision attenuator having 1-dB steps as an artificial signal source. The curve of peak pulse voltage versus chart recorder readings obtained with the diode used in all the following measurements is shown in Fig. 14. A quadratic correction curve can fit the data points to the required accuracy for recorder scale readings between 20 and 100. Gain switching at the oscilloscope can keep the signals within this range.

Spectrometer Test Using Ruby

After all components of the spectrometer were working properly, a ruby rod of laser quality, 1-1/2 in. long by 1/4 in. o.d., was used as a test sample. The pumped-to-unpumped transmission ratio for ruby is well known. (See Refs. 2-4 for data and other references.) A c-axis "0°" ruby rod was used so that a polarizer would not be required, as is the case with YAG. The I_p/I_u ratio was found to be unity at 6070 Å and 4860 Å and was shown to become nearly unity again at 6995 Å. This confirms the observation reported in Refs. 2-4 (Fig. 14) that ordinary ray metastable state absorption is almost equal to the ground state absorption at the 6795 Å $^4A_2 \rightarrow {}^2T_1$ absorption peak. Since the ground state absorption cross section is $\sigma_o(\omega) = 2.5 \times 10^{-21}$ cm^2 at 6795 Å, we concluded that $\sigma^*(\omega) = 2.5 \pm .3 \times 10^{-21}$ cm^2 at the same wavelength. Running with continuous wavelength scan and sampling at intervals of the order of the instrumental resolution makes such structure much more evident than with the course sampling techniques used previously. The agreement at equivalent measuring wavelengths is reassuring and indicates that the automatic scanning spectrometer is performing satisfactorily.

Nd: YAG Metastable State Absorption Spectrum

The energy level diagram of Nd^{3+}: YAG is shown in Fig. 15. The levels below 20,000 cm^{-1} are in accord with those given by Koningstein and Geusic;[5] the levels at shorter wavelengths are from our measurements with the crystal at 296° K, using assignments in best agreement with those of Dieke and Crosswhite.[24] On the right-hand side of Fig. 15 is a wavenumber scale displaced by the wavenumber of the lower of the metastable levels to permit comparison with observed metastable state absorptions. It is clear from inspection of this diagram that there should be very little sharp line absorption from the metastable state at wavelengths shorter than 1μ but that there may be considerable absorption in the 1.6-μ and 1.3-μ regions. It is fortunate for laser operation that there is a mismatch

between the $^4F_{3/2} \longrightarrow {}^4I_{11/2}$ and the $^4F_{3/2} \longrightarrow {}^4G_{9/2}$ transitions so that laser gain should not be reduced by metastable state line absorption.

A laser rod sample having about 1.5 atomic percent of the Y^{3+} ions replaced by Nd^{3+}, 3.8 cm long by 0.635 cm o.d., with flat, parallel polished end faces and fine ground cylindrical surface, was used for the measurements. Cool nitrogen gas flow kept the sample at about 20° C during the series of measurements. Bleaching of ground state absorption lines indicates that only about 3 percent of the population is removed from the ground state under the conditions of the experiment. Higher pump energies did not significantly increase the population of the metastable level, presumably because stimulated "super radiance" rapidly increases the metastable decay rate as population inversion reaches this level. The low metastable state population permitted us to see only the strongest metastable state absorption lines, as listed in Fig. 15. The absorption cross sections listed must be taken as very approximate in absolute value since the estimated standard deviation on metastable state population is 3 percent ±0.5 percent, and the Nd^{3+} concentration of 1.5 percent is taken from the manufacturer's specification, with no specification of tolerances. Furthermore, the lines were all of about the resolution width of the spectrometer (about 3 Å half width), indicating that higher resolution is required for accurate measurement of peak absorption, even at room temperature. The continuous background of metastable state absorption is perhaps the most useful finding of these experiments. The combined metastable absorption cross section at 5600 Å is about 4×10^{-21} cm^2, with only a small wavelength dependence noted.

Decay times of fluorescence and metastable absorption were measured by varying the photomultiplier gate delay from the pump trigger. The results of two such experiments are shown in Fig. 16. Fluorescence decay at 9450 Å from the $^4F_{3/2}$ levels to the highest lying $^4I_{9/2}$ level gives a $^4F_{3/2}$ decay time of 215 μsec. The metastable state absorption time dependence at λ = 9604 Å is comlicated by the superposition of a slight intensity change due to change in YAG rod optical characteristics upon heating by pump flash. The slope of the segment of the curve that is due to metastable state decay, however, agrees well with the fluorescent decay time measurement.

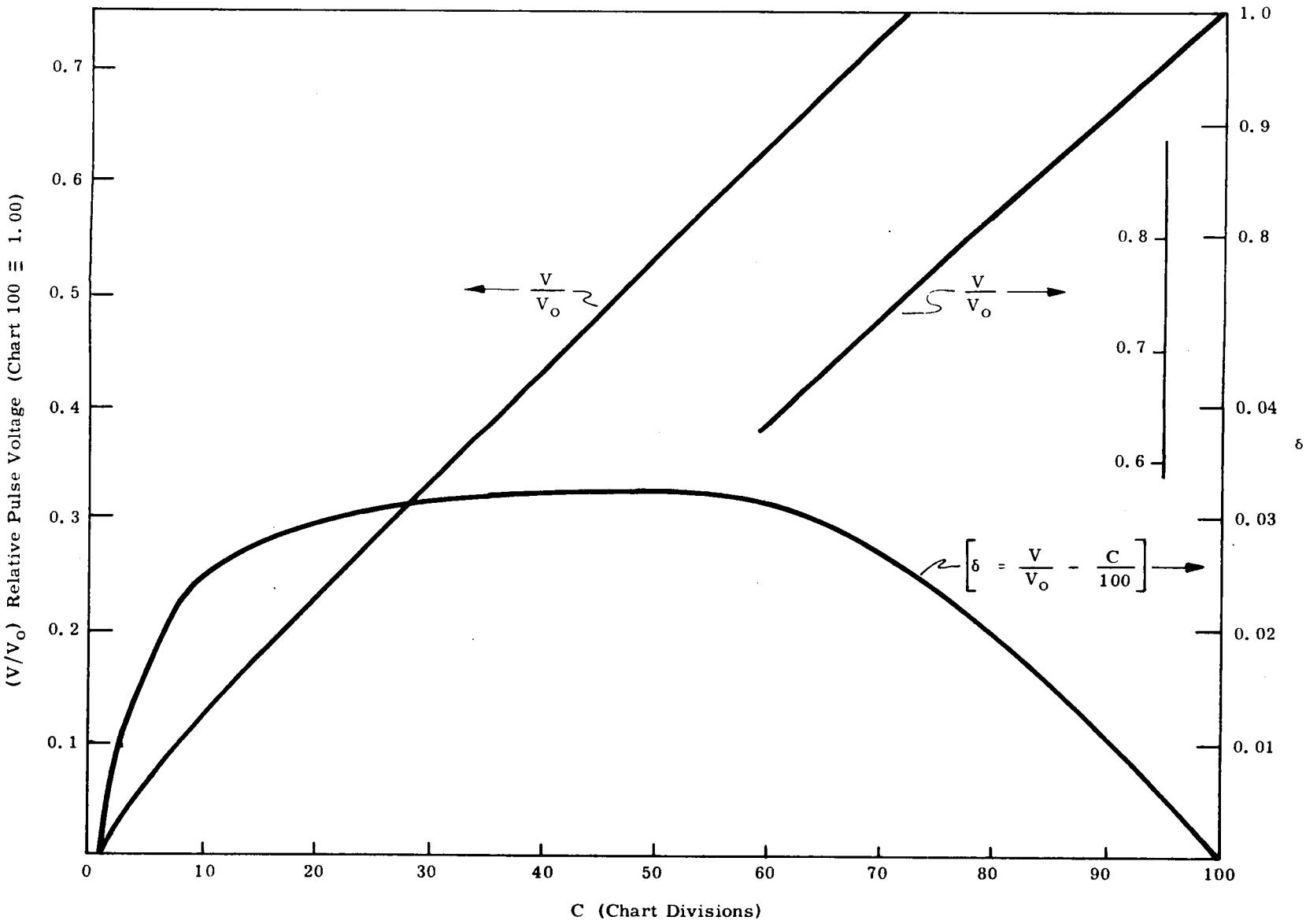

Fig. 14. Chart recorder reading versus peak voltage and correction curve.

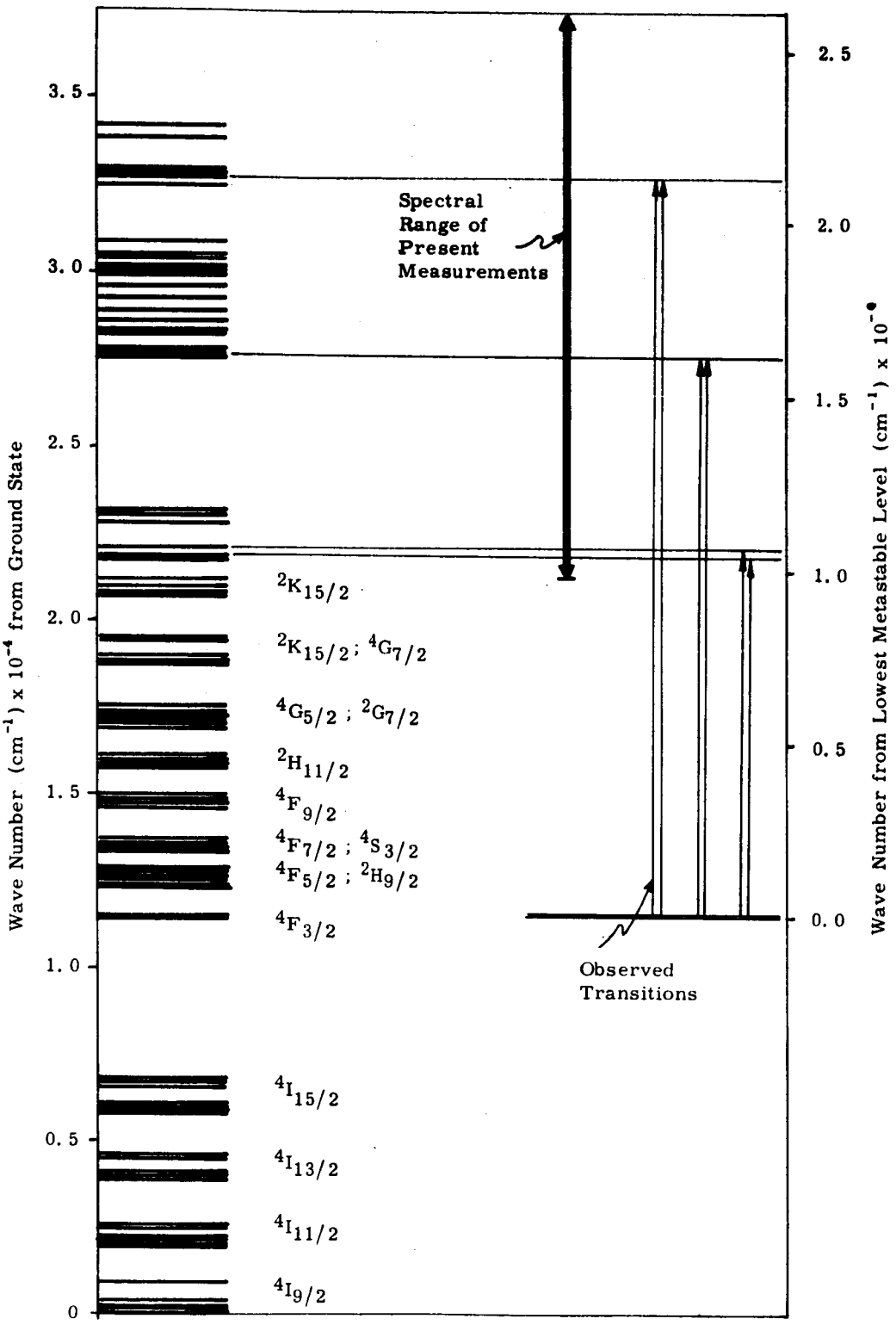

Fig. 15. Energy level diagram of Nd^{3+}:YAG showing observed metastable state absorption.

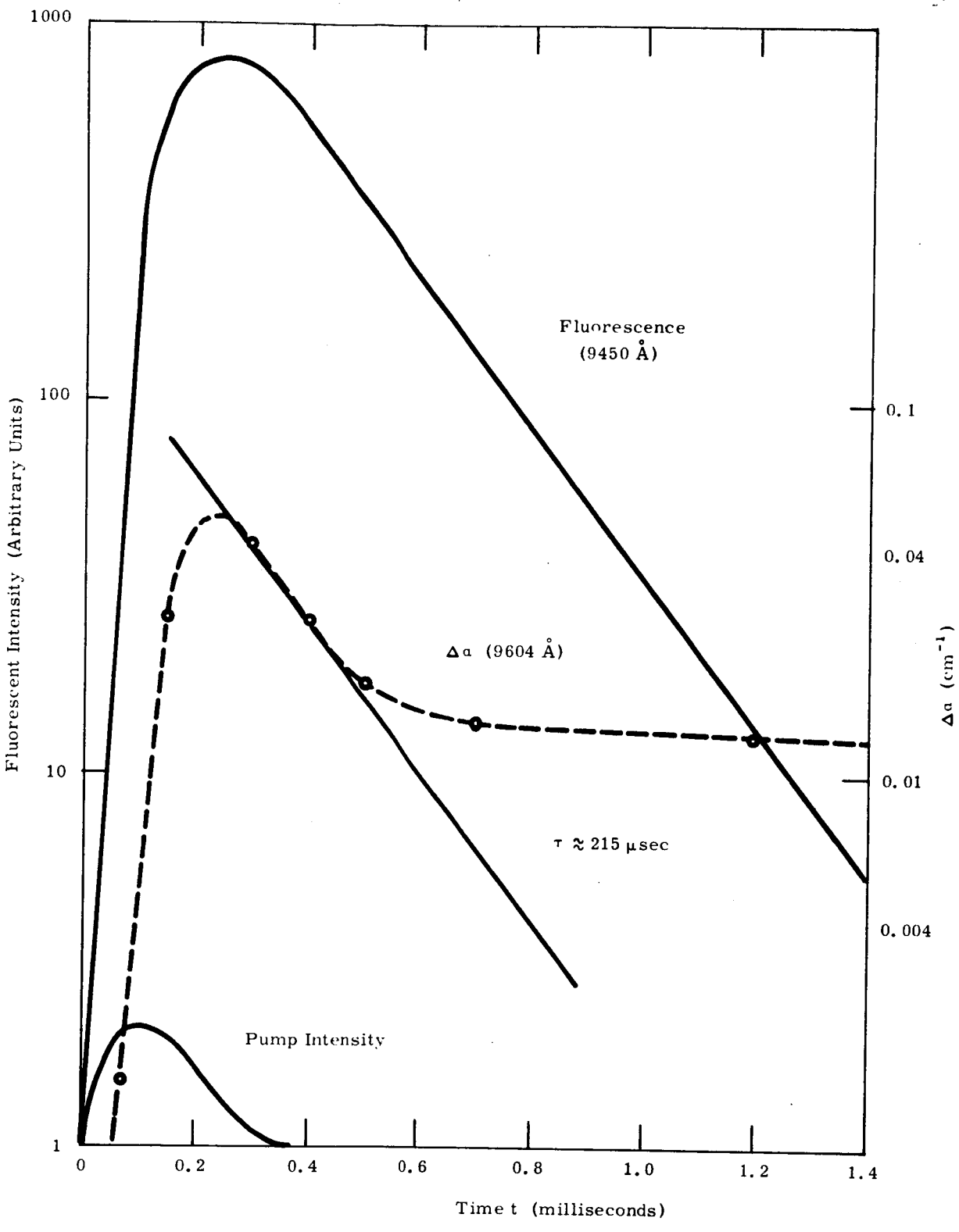

Fig. 16. Time dependence of fluorescence and transient absorption in Nd^{3+}:YAG.

RESULTS AND CONCLUSIONS

CRYSTAL FIELD CALCULATIONS

Each of the possibilities originating from (12 - 14) has been tried for each of the six associations of (E_1, E_2, E_3) with the three observed levels. None could reproduce the three higher levels as the eigenvalues of the W-matrix to any respectable proximity (say ± 20 cm^{-1} or even more). (The g-values of the lowest of the $j = 5/2$ manifold[16] could be the final check if many possibilities qualified on energetic considerations alone, and went unused.) It is to be noted, of course, that the three values (E_1, E_2, E_3) were associated rigidly with the three observed values. It might be said that allowing a relaxation, even in the values of levels of $j = 7/2$, could beget a good fit. But, by that time the intrinsic non-linearity of the equations will make any attempt for a fit overwhelmingly difficult, if not pointless. It seems more reasonable to deduce that the failure of this approach to explain the data is due to some other reasons. They are listed below.

1. The method depended heavily on the ground state doublet structure proposed by Koster and Satz. The zero amplitudes of two state vectors in a total of four made the theoretical simplification possible. But the ground state doublet may very well have a different structure, in which case the workability of this method becomes doubtful.

2. It might be that we failed because the degrees of freedom of the system are 7; i.e., the $j = 7/2$ and $j = 5/2$ manifolds are mixed by the crystal potential. Such an extensive calculation is indeed carried out by Pearson and his collaborators.[17] The ground state they obtain still has the predominantly cubic Γ_7 structure (in the bigger space of the orbits). Their results agree well with the experiment, except for the temperature dependent values of susceptibility. This last factor is rather disconcerting because when one exhausts the whole vector space available to the model, it is imperative for the success of the model that no major disagreement with the experiments is left. It may be that the new susceptibility measurements[18] will clear up this disagreement. Theoretically, on the other hand, the question remains that by the time one is forced to allow mixing of groups of states separated by approximately 10,000 cm^{-1} what is the guarantee that other effects like lattice vibrations and covalent bonds could be

neglected? These effects could drastically change the nature of quantum-states from what one deals with in the simple-minded crystal field theory. It is proposed by some authors[19] that the covalent bond effects are really so strong that the method of crystalline electrostatic potential should not be used. One should instead treat the whole ligand as a unit. We have certainly not touched this crucial question,[20] but our results are not inconsistant with such a rejection of crystal field theory as a quantitative method for dealing with localized electronic states in crystals.

METASTABLE STATE ABSORPTION

The results of Nd^{3+}: YAG metastable state absorption measurements completed under the present contract are the observation of sharp line absorption from the metastable state to certain higher lying states also observed in ground state absorption spectra, in addition to a continuum of metastable state absorption extending from approximately 6000 Å into the ultraviolet. The resolution of the present experiment (~3 Å) was not adequate to permit accurate measurement of sharp line absorption cross sections, but the combined continuum absorption at 5600 Å is about 4×10^{-21} cm^2 and increases gradually toward the ultraviolet. Since very little useful pumping is done at wavelengths shorter than 5000 Å, and the metastable state absorption continuum at those wavelengths contributes to crystal heating, removal of shorter wavelengths from the pump light is recommended for continuous wave Nd^{3+}: YAG lasers in cases where efficiency and high power output are important.

The present metastable state absorption spectrometer could be improved in a number of ways. The most significant improvement would come from a higher resolution monochromator having higher scattered light rejection. Another improvement would be the use of metal substrate photocathodes, which would permit higher peak intensities to be measured, reducing photon statistical noise in the short pulse detection mode.

It is recommended that the measurements be extended to longer wavelengths in order to determine the need for more effective filtering of long wavelength ($> 0.9\ \mu$) pump light from Nd : YAG lasers. It would also be of interest to study other optically pumped laser materials in this way. The technique should certainly be used to supplement conventional spectroscopic examination of potential laser materials since the method yields considerably more information about the characteristics of a material under optical pumping.

REFERENCES

1. E. G. Brock, F. C. Unterleitner, Y. C. Kiang, and J. F. Stephany, "Laser Modulation at the Atomic Level," Final Report, Contract NASw 1008, February 1966.

2. T. Kushida, "Absorption Spectrum of Optically Pumped Ruby," J. Phys. Soc. Japan 21, 1331 (1966).

3. Y. C. Kiang, J. F. Stephany, and F. C. Unterleitner, "Visible Spectrum Absorption Cross Section of the Metastable ^2E State of Cr^{3+} in Ruby," J. Quantum Elec.

4. F. C. Unterleitner and Y. C. Kiang, "Optical Interactions in Ruby Lasers," Final Report to AFCRL, Contract AF 19(628)-5810, AFCRL-67-0194, 28 February 1967.

5. J. A. Koningstein and J. E. Geusic, "Energy Levels and Crystal-Field Calculations of Neodymium in Yttrium Aluminum Garnet," Phys. Rev. 136, A 711 (1964).

6. H. Bethe, Ann. Physik 3, 133 (1929).

7. M. Sachs, Solid State Theory (Mc Graw-Hill Inc., 1963), Chap. IV.

8. R. A. Buchanan, K. A. Wickersheim, J. J. Pearson, and G. F. Herrman, Conference on "Optical Properties of Ions in Crystals," Johns Hopkins University, September 1966.

9. M. T. Hutchings and W. P. Wolf, J. Chem. Phys. 41, 617 (1964).

10. D. L. Wood, J. Chem. Phys. 39, 1671 (1963).

11. G. F. Koster and H. Statz, Proceedings of the First International Conference on Paramagnetic Resonance (Academic Press, New York, 1963), pp. 368-69.

12. G. F. Koster, J. O. Dimmock, R. G. Wheeler, and H. Statz, Properties of the Thirty-two Point Groups (M. I. T. Press, Cambridge, Mass., 1963).

13. W. Low, Advance in Solid State Physics (Academic Press, New York and London, 1960), Supplement 2.

14. J. H. Van Vleck, "Proceedings of the International Conference on Magnetism and Crystallography," published by the Physical Society of Japan, Vol. 17, Supplement B-1, p. 352, March 1962.

15. R. Pappalardo and D. L. Wood, J. Chem. Phys. 33, 1734 (1960).

16. H. M. Crosswhite, unpublished.

17. J. J. Pearson, G. F. Herrman, K. A. Wickersheim, and R. A. Buchanan, Lockheed Palo Alto Research Lab., private communication (1967).

18. Mentioned by Prof. Van Vleck in a private communication (1967).

19. C. K. Jorgenson, R. Pappalardo, and H. Schmidtke, J. Chem. Phys. 39, 1422 (1963).

20. J. H. Van Vleck, J. Phys. Chem. Solids 27, 1047 (1966).

21. S. Geschwind, G. E. Devlin, R. L. Cohen, and S. R. Chinn, "Orbach Relaxation and Hyperfine Structure in the Excited $\overline{E}$ (^2E) State of Cr^{3+} in Al_2O_3," Phys. Rev. 137, A1087 (1965).

22. C. A. Hutchison, Jr. and B. W. Mangum, "Paramagnetic Resonance Absorption in Naphthalene in Its Phosphorescent State," J. Chem. Phys. 34, 908 (1961).

23. P. L. Scott and C. D. Jeffries, "Spin-Lattice Relaxation in Some Rare Earth Salts," Phys. Rev. 127, 32 (1962).

24. G. H. Dieke and H. M. Crosswhite, "The Spectra of Doubly and Triply Ionized Rare Earths," Appl. Optics 2, 675 (1963).